Differentiation of crescent-forming kidney progenitor cells into podocytes attenuates severe glomerulonephritis in mice

(Article begins on next page)

16 August 2024

KIDNEY DISEASE

Differentiation of crescent-forming kidney progenitor cells into podocytes attenuates severe glomerulonephritis in mice

Maria Elena Melica[1,2], Giulia Antonelli[1,2], Roberto Semeraro[3], Maria Lucia Angelotti[1,2], Gianmarco Lugli[2,4], Samuela Landini[4], Fiammetta Ravaglia[2], Gilda La Regina[2], Carolina Conte[1,2], Letizia De Chiara[1,2], Anna Julie Peired[1,2], Benedetta Mazzinghi[4], Marta Donati[4], Alice Molli[4], Stefanie Steiger[5], Alberto Magi[6], Niccolò Bartalucci[7], Valentina Raglianti[2,4], Francesco Guzzi[2,4], Laura Maggi[3], Francesco Annunziato[3], Alexa Burger[8], Elena Lazzeri[1,2], Hans-Joachim Anders[5], Laura Lasagni[1,2]*†, Paola Romagnani[1,2,4]*†

Crescentic glomerulonephritis is characterized by vascular necrosis and parietal epithelial cell hyperplasia in the space surrounding the glomerulus, resulting in the formation of crescents. Little is known about the molecular mechanisms driving this process. Inducing crescentic glomerulonephritis in two Pax2Cre reporter mouse models revealed that crescents derive from clonal expansion of single immature parietal epithelial cells. Preemptive and delayed histone deacetylase inhibition with panobinostat, a drug used to treat hematopoietic stem cell disorders, attenuated crescentic glomerulonephritis with recovery of kidney function in the two mouse models. Three-dimensional confocal microscopy and stimulated emission depletion superresolution imaging of mouse glomeruli showed that, in addition to exerting an anti-inflammatory and immunosuppressive effect, panobinostat induced differentiation of an immature hyperplastic parietal epithelial cell subset into podocytes, thereby restoring the glomerular filtration barrier. Single-cell RNA sequencing of human renal progenitor cells in vitro identified an immature stratifin-positive cell subset and revealed that expansion of this stratifin-expressing progenitor cell subset was associated with a poor outcome in human crescentic glomerulonephritis. Treatment of human parietal epithelial cells in vitro with panobinostat attenuated stratifin expression in renal progenitor cells, reduced their proliferation, and promoted their differentiation into podocytes. These results offer mechanistic insights into the formation of glomerular crescents and demonstrate that selective targeting of renal progenitor cells can attenuate crescent formation and the deterioration of kidney function in crescentic glomerulonephritis in mice.

INTRODUCTION

Crescentic glomerulonephritis encompasses a group of diverse disorders characterized by hyperplasia of parietal epithelial cells (PECs) in the space surrounding the glomerulus (so-called crescents) as the main histopathological lesion at kidney biopsy (1, 2). Crescents are frequently associated with a rapid decline in kidney function referred to as rapidly progressive glomerulonephritis (1, 2). Anti-neutrophil cytoplasmic antibody-associated small vessel vasculitis is the most frequent underlying diagnosis (3), but crescents form also in cryoglobulinemic vasculitis, anti–glomerular basement membrane (GBM) disease (4), lupus nephritis (LN), and other forms of immune complex glomerulonephritis. Crescents involving more than 50% of glomeruli are associated with poor prognosis in terms of kidney function and patient survival.

Crescent formation is the consequence of diverse upstream pathomechanisms that have a shared response involving the specific activation of PECs. PECs normally reside along the Bowman capsule of the glomerulus and represent in part renal progenitor cells that are kept quiescent through a humoral feedback loop by differentiated podocytes of the intact glomerular filtration barrier (1, 2, 5, 6). Podocyte injury disrupts this feedback loop and activates PECs through surface glycoproteins, such as CD44 (7) and CD9 (8), that promote their activation, migration, and proliferation (9, 10). Renal progenitor cells have a high survival capacity (11) and proliferative potential (11), and renal progenitor cell markers are observed in crescents from patients with different types of glomerulonephritis (12).

On the basis of similarities between stem cell niches of bone marrow and kidney (13), we hypothesized that crescents result from monoclonal expansion of a single renal progenitor cell clone conceptually similar to monoclonal diseases originating from hematopoietic stem cells. According to this analogy, we further hypothesized that drugs for treating monoclonal diseases of the hematopoietic stem cells by enforcing their terminal differentiation could also attenuate crescentic glomerulonephritis (6, 14, 15).

[1]Excellence Center for Research, Transfer and High Education for the Development of DE NOVO Therapies (DENOTHE), University of Florence, Florence 50139, Italy. [2]Department of Experimental and Clinical Biomedical Sciences "Mario Serio", University of Florence, Florence 50139, Italy. [3]Department of Experimental and Clinical Medicine, University of Florence, Florence, Italy. [4]Nephrology and Dialysis Unit, Meyer Children's Hospital, Florence 50139, Italy. [5]Division of Nephrology, Medizinische Klinik and Poliklinik IV, Klinikum der LMU München, Munich 80336, Germany. [6]Department of Information Engineering, University of Florence, Florence, Italy. [7]Department of Experimental and Clinical Medicine, CRIMM, Center Research and Innovation of Myeloproliferative Neoplasms, AOUC, University of Florence, Florence 50139, Italy. [8]Section of Developmental Biology, Department of Pediatrics, University of Colorado Anschutz Medical Campus, Aurora, CO 80045, USA.
*Corresponding author. Email: paola.romagnani@unifi.it (P.R.); laura.lasagni@unifi.it (L.L.)
†These authors contributed equally to this work.

RESULTS

### Crescents derive from Pax2+ progenitor cells of the glomerular Bowman capsule

To evaluate the contribution of renal progenitor cells among the PECs to the generation of crescents, we used *Pax2.rtTA;TetO.Cre;mT/mG* conditional transgenic reporter mice that enabled genetic labeling

of progenitor cells with green fluorescent protein (GFP) and lineage tracing (*6*). Following transgene induction by doxycycline administration, all Pax2^{+} progenitor cells among the PECs were marked in green (fig. S1A). After a washout period (*16*), we induced crescentic glomerulonephritis by intravenous injection of sheep anti-GBM serum (fig. S1B). On day 7, we observed sheep immunoglobulin G (IgG) deposits in the glomeruli (fig. S1C). Periodic acid–Schiff (PAS) staining revealed focal segmental capillary loop necrosis and crescent-like proliferation of PECs in the Bowman space, i.e., the empty space around the glomerular tuft that collects the filtrate (Fig. 1A) in 37.7 ± 3.0% of the glomeruli (Fig. 1B). Glomerular damage was associated with a rapid increase in albuminuria at day 1, which declined in the following days remaining higher than in healthy mice at day 7 (Fig. 1C). Proteinuria was accompanied by a loss of kidney function, shown by a drop in glomerular filtration rate (GFR) (Fig. 1D) and by an increase in blood urea nitrogen (BUN) (Fig. 1E), which together indicated severe glomerulonephritis. Lineage tracing experiments and three-dimensional (3D) microscopic confocal analysis showed that the Pax2^{+} subset of PECs expanded circumferentially in the Bowman capsule and largely constituted the glomerular crescents (Fig. 1, F to H). Together, the data indicate that crescents may originate from immature Pax2^{+} cells among the PECs that then proliferate extensively.

Crescents originate from clonal expansion of single Pax2^{+} progenitor cells

The origin of crescents from proliferation of Pax2^{+} progenitor cells suggested a possible similarity to disorders induced by uncontrolled clonal proliferation or differentiation arrest of a subpopulation of hematopoietic stem cells, such as myelodysplastic syndrome, leukemia, or myelofibrosis (*14*, *15*). To evaluate the possibility that crescents could be clonal lesions, we used the *Pax2.rtTA;TetO.Cre;Rosa26. Confetti* conditional transgenic mouse model that allowed clonal lineage tracing by genetical labeling of individual Pax2^{+} cells with one of four fluorescent proteins (fig. S1D) (*6*). To detect the entire crescentic lesion, we performed z-stack analysis and 3D reconstructions of glomeruli in 30-μm-thick sections (Fig. 2, A to D) (*5*). Quantification of 3D analysis showed that in healthy mice, the number of Pax2^{+} cells per glomerulus was 4.6 ± 0.2, whereas in mice with crescentic glomerulonephritis Pax2^{+} cells expanded to 18.9 ± 1.8 per
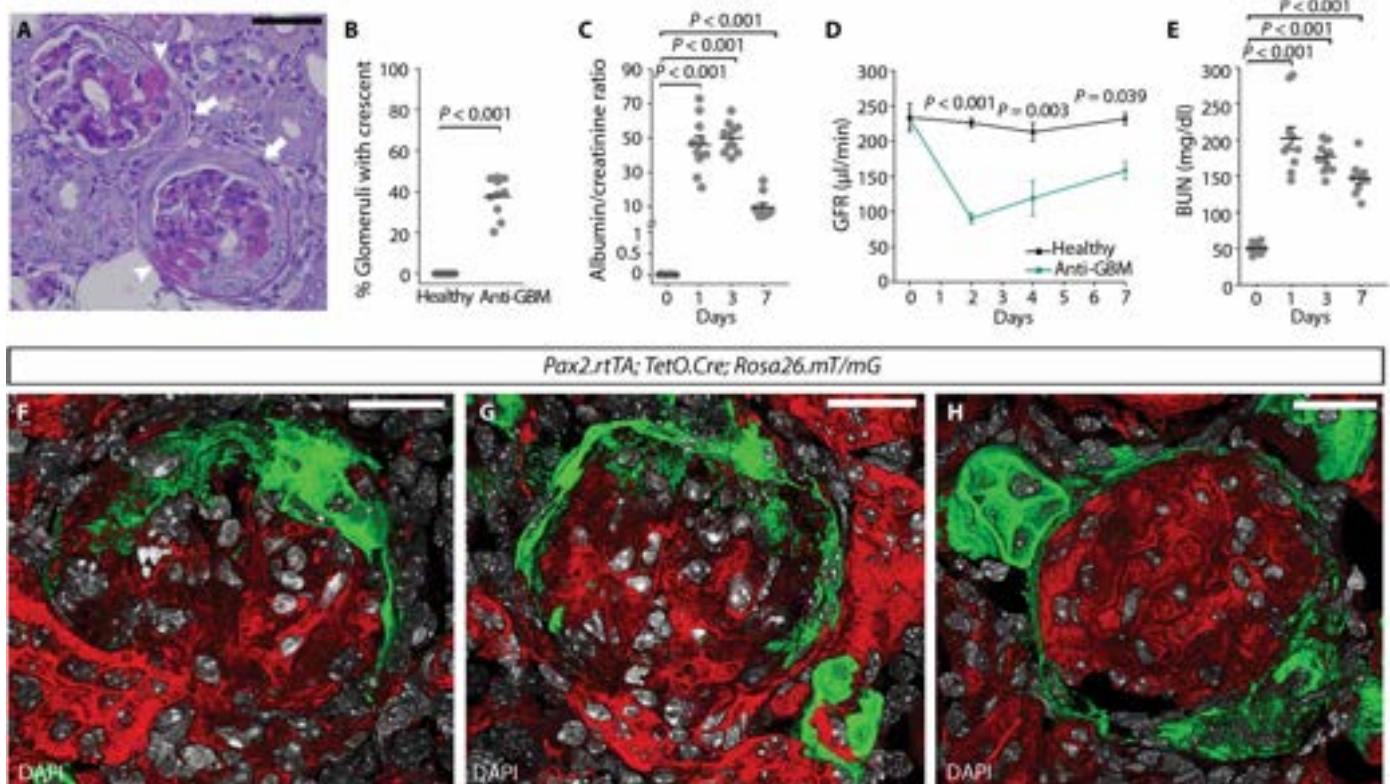
Fig. 1. Crescents are generated from renal progenitor cells. (**A**) Representative image of a PAS-stained kidney section from a mouse with crescentic glomerulonephritis induced by injection of anti–glomerular basement membrane (GBM) antibodies. Crescents (white arrows) and glomerulosclerosis (white arrowheads) are indicated. Scale bar, 50 μm. (**B**) Quantification of glomeruli with crescents in PAS-stained kidney sections from anti-GBM–treated mice at day 7 after injection with anti-GBM serum (*n* = 10). (**C**) Assessment of the albumin/creatinine ratio in urine from anti-GBM–treated mice (*n* = 10). (**D**) Glomerular filtration rate (GFR) over time in healthy mice and in mice after injection of anti-GBM serum. Data are means ± SEM (healthy mice, *n* = 5; anti-GBM–treated mice, *n* = 5). (**E**) Blood urea nitrogen (BUN) values over time in anti-GBM–treated mice (*n* = 10). (**F** to **H**) 3D reconstruction of glomeruli showing Pax2-tracked hyperplastic lesions (green) in kidney sections from the *Pax2.rtTA;TetO. Cre;Rosa26.mT/mG* mouse model of crescentic glomerulonephritis at day 7 after injection with anti-GBM serum. 4′,6-Diamidino-2-phenylindole (DAPI) (white) was used to counterstain nuclei. Scale bar, 20 μm. In (F) to (H), signals for fluorescent *mT/mG* proteins are GFP (green) and tdTomato (red). In dot plots (B), (C), and (E), bars indicate mean values. Individual scores are shown. Statistical significance was calculated by Mann-Whitney test (B, C, and E) or two-way analysis of variance (ANOVA) with Bonferroni post hoc test (D); numbers on graph represent *P* values.
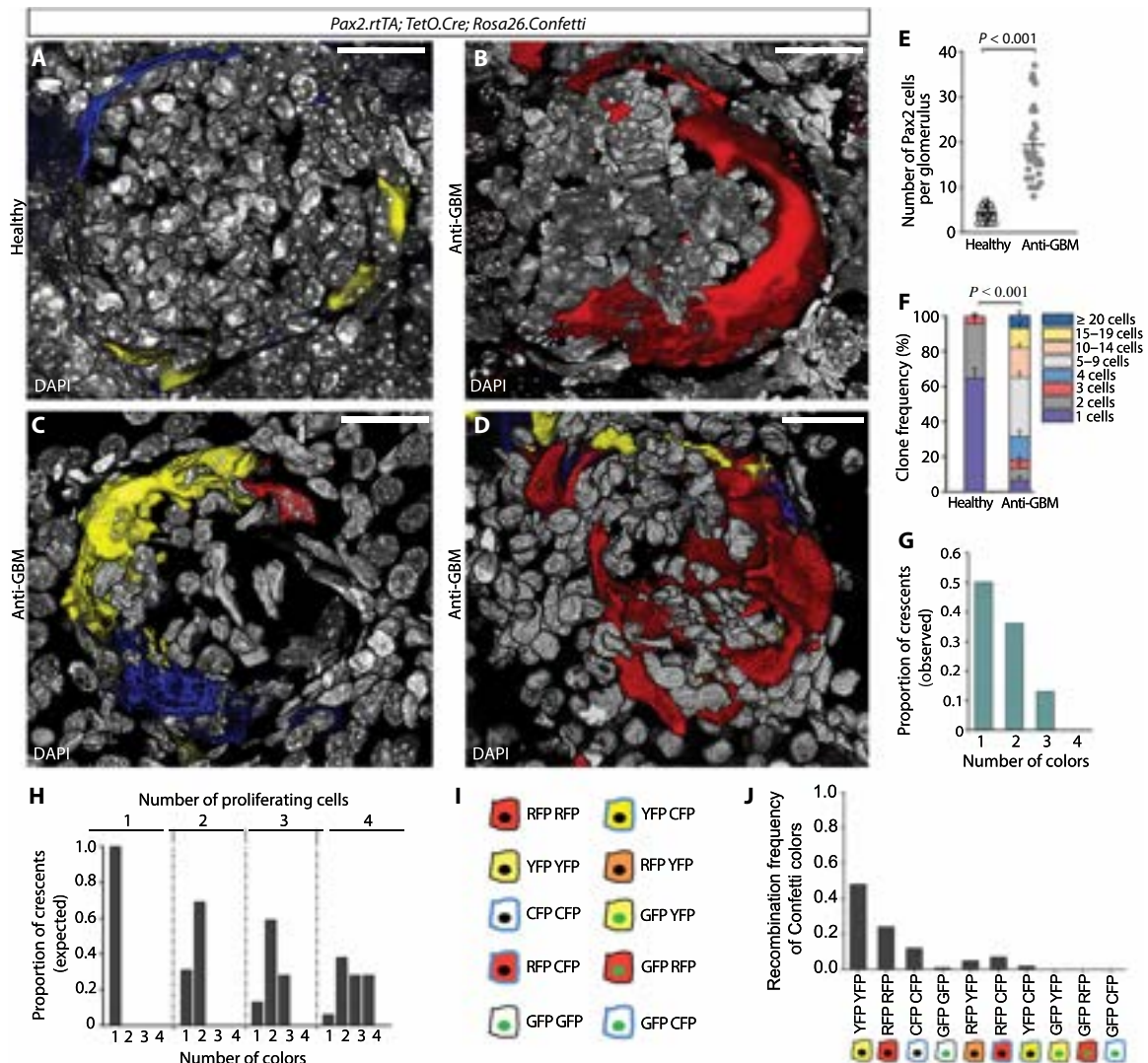
Fig. 2. Crescents are generated by clonal proliferation of single renal progenitor cells. (**A** to **D**) 3D reconstruction of representative glomeruli of healthy *Pax2.rtTA;TetO. Cre;Rosa26.Confetti* mice (A) and of anti-GBM–treated mice with crescentic glomerulonephritis (B to D). DAPI (white) was used to counterstain nuclei. Scale bars, 20 μm. (**E**) Dot plot of the 3D analysis presented in (A) to (D) showing the number of Pax2^{+} cells per glomerulus in healthy mice (*n* = 9) and in anti-GBM–treated mice (*n* = 6) at 7 days after injection of anti-GBM serum. (**F**) Clone frequency analysis of Pax2^{+} cells in glomeruli of healthy mice (*n* = 9) and anti-GBM–treated mice (*n* = 6) at day 7 after injection of anti-GBM serum. Data are means ± SEM. (**G**) Bar chart showing the number of colors of the fluorescent Confetti reporter observed per crescent in anti-GBM– treated mice (*n* = 6). (**H**) Bar chart showing the theoretical distribution of colors of the fluorescent Confetti reporter per crescent resulting from proliferation of one, two, three, or four Pax2^{+} cells labeled at the recombination frequency observed in animals after induction of expression of the fluorescent Confetti reporter by doxycycline administration. (**I**) Color combinations generated by recombination of the four possible fluorescent reporter proteins (nuclear GFP, membrane-associated CFP, cytoplasmic RFP, and cytoplasmic YFP) in mice homozygous for the R26R-Confetti allele, after induction by doxycycline administration to *Pax2.rtTA;TetO.Cre;Rosa26.Confetti* mice. (**J**) Bar chart showing the proportion of each Confetti color in 3D reconstructed glomeruli of healthy mice after induction by doxycycline (*n* = 9 mice). In (A) to (D), signals for fluorescent *Confetti* proteins are GFP (green), CFP (cyan), RFP (red), and YFP (yellow). In dot plot (E), bars indicate mean values. Individual scores are shown. Statistical significance was calculated by Mann-Whitney test (E and F).

glomerulus (*P* < 0.001) (Fig. 2E). Clone frequency analysis revealed that more than 60% of clones were bigger than 5 cells, with a maximum clone size of 25 cells (Fig. 2F). In particular, 50% of crescents showed a single color indicating clonality, 36% showed two colors, and only 13% showed three colors (Fig. 2G). The observed color frequency matched the theoretically expected color pattern generated if no more than one to two Pax2^{+} cells proliferated to generate a crescent (Fig. 2H), calculated on the basis of the recombination frequency of each color observed in glomeruli of healthy mice

(Fig. 2, I and J). Together, these results show that crescents derive from clonal proliferation of single Pax2^{+} PECs.

Panobinostat attenuates crescentic glomerulonephritis

The origin of crescents from clonal proliferation of single progenitor cells suggested a possible pathogenic similarity to proliferative hematopoietic stem cell disorders (*17*). Therefore, we examined the effect of three drugs successfully used for treating acute myeloid leukemia and primary myelofibrosis by inhibiting the clonal expansion

of the pathogenic hematopoietic stem cell clone, the two histone deacetylase inhibitors panobinostat and givinostat and the Janus kinase 1/2 (JAK1/2) inhibitor ruxolitinib (*17–19*). First, we induced crescentic glomerulonephritis in *Pax2.rtTA;TetO.Cre;mT/mG* mice and *Pax2.rtTA;TetO.Cre;Rosa26.Confetti* mice by injection of anti-GBM serum, and then we treated the animals with one of the three compounds for 6 days starting 18 hours after injection. Animals were sacrificed at day 7 (fig. S1E). Panobinostat treatment decreased the number of crescents in comparison to the vehicle-treated group at day 7 after treatment (*P* = 0.005; Fig. 3, A, B, E, and F), whereas no effects were
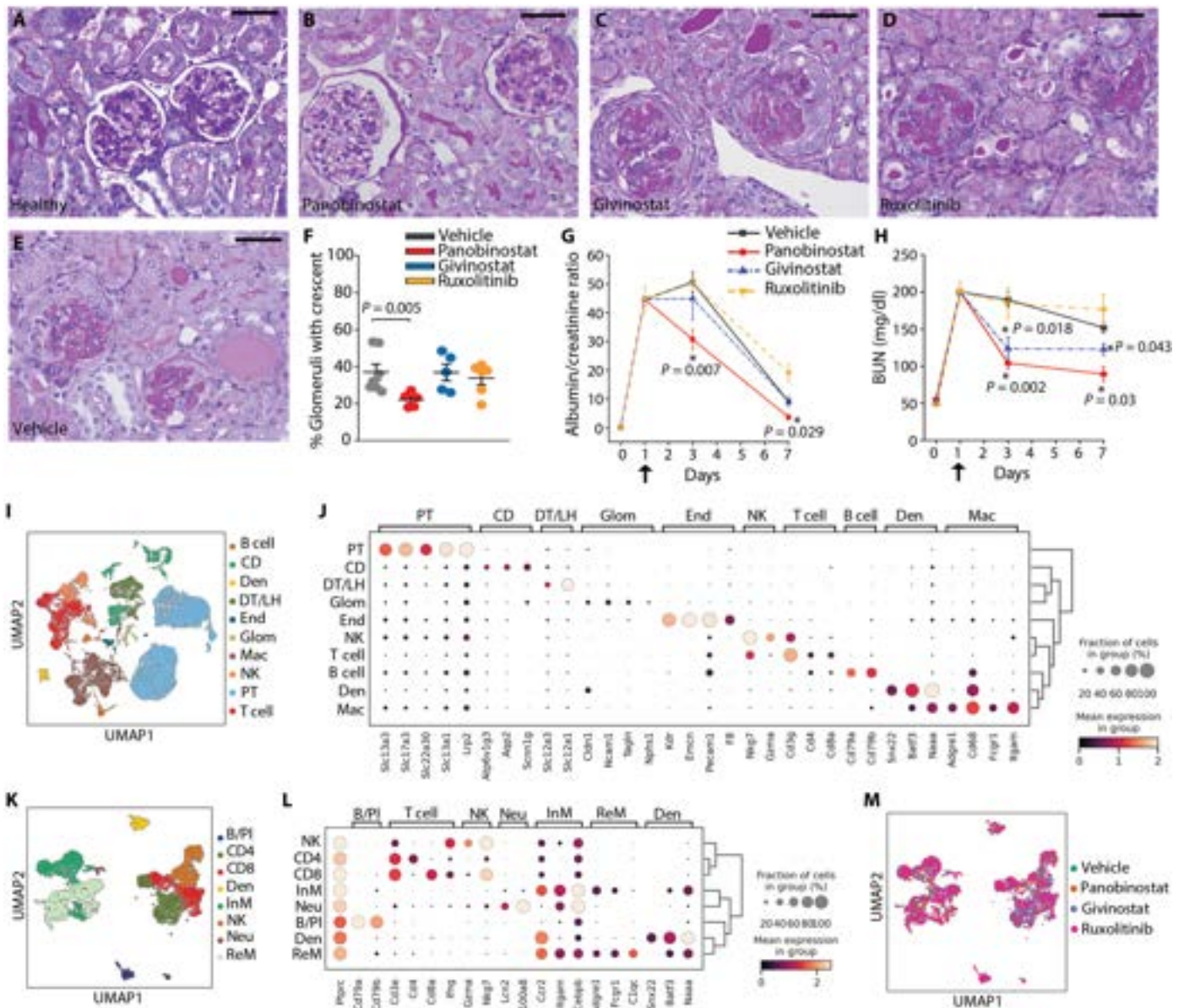
Fig. 3. Panobinostat attenuates crescentic glomerulonephritis independently from its anti-inflammatory effect. (**A** to **E**) Representative images of PAS-stained kidney sections from a healthy mouse (A) and from mice at 7 days after injection of anti-GBM serum that were treated with (B) panobinostat, (C) givinostat, (D) ruxolitinib, or (E) vehicle. Scale bars, 50 μm. (**F**) Percentage of glomeruli with crescents at day 7 after injection of anti-GBM serum in the three experimental groups of mice (panobinostat, *n* = 5; givinostat, *n* = 5; ruxolitinib, *n* = 6) and in the vehicle control group (*n* = 7). (**G**) Time course of changes in the urine albumin/creatinine ratio and (**H**) changes in BUN values determined in the four groups of mice (vehicle, *n* = 7; panobinostat, *n* = 5; givinostat, *n* = 5; ruxolitinib, *n* = 6). Data are means ± SEM. Black arrows indicate the starting point for drug treatment. (*) significance of panobinostat versus vehicle. (**I**) Uniform manifold approximation and projection (UMAP) visualization of cluster distribution of kidney cells in mouse kidneys derived from mice treated with vehicle (*n* = 2), panobinostat (*n* = 2), givinostat (*n* = 2), and ruxolitinib (*n* = 2). (**J**) Dot plot displaying the representative marker genes of the clusters shown in (I). (**K**) UMAP visualization of cluster distribution of immune cells in mouse kidneys derived from mice treated with vehicle (*n* = 2), panobinostat (*n* = 2), givinostat (*n* = 2), and ruxolitinib (*n* = 2). (**L**) Dot plot displaying the representative marker genes of the clusters shown in (K). (**M**) UMAP visualization of immune cells in mouse kidneys colored according to drug treatment. CD, collecting ducts; Den, dendritic cells; DT/LH, distal tubule and loop of Henle; End, endothelial cells; Glom, glomerular cells; Mac, macrophages; NK, natural killer cells; PT, proximal tubule; B/Pl, B cells and plasma cells; InM, infiltrating macrophages; Neu, neutrophils; ReM, resident macrophages. In dot plot in (F), bar indicates mean values. Individual scores are shown. Statistical significance was calculated by Mann-Whitney test (F to H).

observed in animals receiving givinostat or ruxolitinib (Fig. 3, C to F). Consistently, the albumin/creatinine ratio was improved in animals treated with panobinostat in comparison to the vehicle-treated group, at both day 3 ($P = 0.007$) and day 7 after treatment ($P = 0.029$) (Fig. 3G). Likewise, panobinostat induced recovery of excretory kidney function, and a small effect was observed with givinostat, as shown by improvement of BUN (Fig. 2H). By contrast, no effect was observed with ruxolitinib (Fig. 3H). The doses of givinostat and ruxolitinib were sufficient to block their targets as demonstrated respectively by an increase in lysine 9–acetylated histone H3 (fig. S1F) and reduction in phosphorylated signal transducer and activator of transcription 3 (STAT3) (fig. S1) in comparison to vehicle-treated mice. These results show that panobinostat can attenuate crescent formation, ameliorate proteinuria, and improve excretory kidney function.

Panobinostat promotes the generation of new podocytes
To establish how panobinostat could improve proteinuria and BUN, we performed single-cell RNA sequencing (scRNAseq) on kidney samples obtained from mice with crescentic glomerulonephritis treated with panobinostat and compared it with those treated with givinostat or ruxolitinib (Fig. 3, I to M, and figs. S2 to S4). We first performed an unbiased evaluation to identify genes more differentially modulated among immune system components by panobinostat in comparison to vehicle control, givinostat, or ruxolitinib (Fig. 3, I to M). We did not observe any effect that was specific for panobinostat (fig. S2A). Likewise, we observed no panobinostat-specific effect on the expression of molecules reported in the context of crescentic glomerulonephritis in the literature (fig. S3A) (1, 20–28). Because macrophages have important roles in the pathogenesis of crescentic glomerulonephritis, we further analyzed the effect of panobinostat, givinostat, or ruxolitinib on the expression of major histocompatibility complex class II (MHCII), CD86, CD80, CD40, and interleukin-6 (IL-6) as well as on the phagocytic capacity in murine bone marrow–derived macrophages (fig. S3, B to G). We did not observe any effect specific to panobinostat, suggesting that the three drugs elicited similar anti-inflammatory and immunosuppressive properties. However, only panobinostat strongly reduced proteinuria and induced recovery of excretory kidney function in vivo, so the consistent anti-inflammatory effects of the three compounds cannot serve as an explanation for the differences among the three drugs and other unique properties of panobinostat must apply.

We then further evaluated the effect of panobinostat on resident kidney cells. Similar to what we had observed for the immune system, there was no apparent panobinostat-specific effect on tubular, endothelial, and glomerular kidney cells using an unbiased evaluation (fig. S4A) or when checking the expression of molecules with a reported role in crescentic glomerulonephritis in the literature (fig. S4B) (1, 20–28). To further evaluate the effect of panobinostat on kidney tubules, we used *Pax8.rtTA;TetO.Cre;FUCCI2aR* mice (fig. S5A), which allowed us to track all tubular cells and their cell cycle phases via the fluorescent ubiquitin-based cell cycle indicator (FUCCI2aR) reporter (11). We observed no changes in the total number of tubular cells after treatment with panobinostat, suggesting no effect of panobinostat on tubular cell viability or proliferation (fig. S5B).

Last, we further explored the effects of panobinostat on resident kidney glomerular cells. In the glomerulus, panobinostat reduced fibrin deposition at day 7 of treatment, whereas no effect was observed at day 3 of treatment (fig. S6, A and B). Consistently, quantification of glomerular injury in PAS-stained mouse kidney sections demonstrated that panobinostat treatment reduced the percentage

of injured glomeruli at day 7 of treatment in comparison to vehicle-treated mice (fig. S6, C and D). By performing 3D analysis on kidneys of *Pax2.rtTA;TetO.Cre;R26.mT/mG* mice, we observed smaller crescents in those treated for 7 days with panobinostat in comparison to vehicle (Fig. 4, A to D). This was associated with a reduction of proliferating Pax2-labeled renal progenitor cells within crescents (fig. S7, A and B) and with the appearance of Pax2-derived GFP$^+$ cells inside the glomerular tuft showing morphological features of podocytes, such as primary and secondary foot processes (Fig. 4, B and C). In a time-course analysis, Pax2-derived GFP$^+$ cells appeared first as mostly localized in the Bowman space, then moving toward the glomerular tuft and starting to express synaptopodin at day 3 of treatment, and later engrafting into the tuft at day 7 of treatment (fig. S7, C to I). Upon tissue clearing and staining with anti-synaptopodin and anti-GFP antibodies, we confirmed the reduction in crescent dimensions (Fig. 4, E to I) and observed a concomitant increase in glomeruli containing Pax2-derived podocytes clearly engrafted within the glomerular tuft after treatment with panobinostat (Fig. 4, F to J, and movie S1). Overall, panobinostat treatment resulted in a reduction in the ratio between glomeruli with crescents and glomeruli containing new podocytes ($P < 0.001$) (Fig. 4K). Last, we obtained pure primary cultures of mouse Pax2-labeled renal progenitor cells by sorting GFP$^+$ cells from *Pax2.rtTA;TetO.Cre;R26.mT/mG* mice (Fig. 4, L and M, and fig. S8, A and B). scRNAseq showed that, after treatment with panobinostat, primary cultures of mouse GFP$^+$ renal progenitor cells up-regulated podocyte markers (Fig. 4, N and O). These data suggest that panobinostat reduced crescent formation and promoted de novo generation of podocytes.

Panobinostat improves 3D glomerular structure and restores slit diaphragm integrity
To gain further insight into how panobinostat influenced the integrity of the glomerular filtration barrier, we used stimulated emission depletion (STED) superresolution microscopy imaging for podocin (NPHS2), a slit diaphragm component, in optically cleared mouse kidney tissues to produce volumetric representations of the glomerular slit ultrastructure at the nanometer scale (29). 3D rendering of confocal z stacks showed the complex slit diaphragm structure with interdigitating foot processes in healthy glomeruli (Fig. 5, A and B) but a simplified structure in mice injected with anti-GBM serum that developed crescentic glomerulonephritis (Fig. 5, C and D). This was consistent with foot process effacement or podocyte loss in crescent areas and in areas of podocytes surrounding the crescents. Podocyte loss and reduction of foot process density were less evident in kidney sections from panobinostat-treated animals (Fig. 5, E and F). Overall, panobinostat treatment resulted in an increase in glomeruli with an improved barrier integrity from 28.27.0% ± 5.68 to 72.52% ± 3.44 ($P = 0.029$) (Fig. 5G). Quantitative analysis showed that panobinostat treatment increased the filtration slit density as a marker of podocyte foot process density in comparison to vehicle-treated mice ($P = 0.0003$) (Fig. 5, H to J). These results suggest that panobinostat halts the hyperplasia of immature PECs and instead induces their differentiation into new mature podocytes that repair the injured glomerular filtration barrier and favor restoration of the slit diaphragm density in mice with crescentic glomerulonephritis.

### Panobinostat retains its renoprotective capacity after treatment delay
We then evaluated the capacity of panobinostat to exert a renoprotective effect once the injury had already been established and its
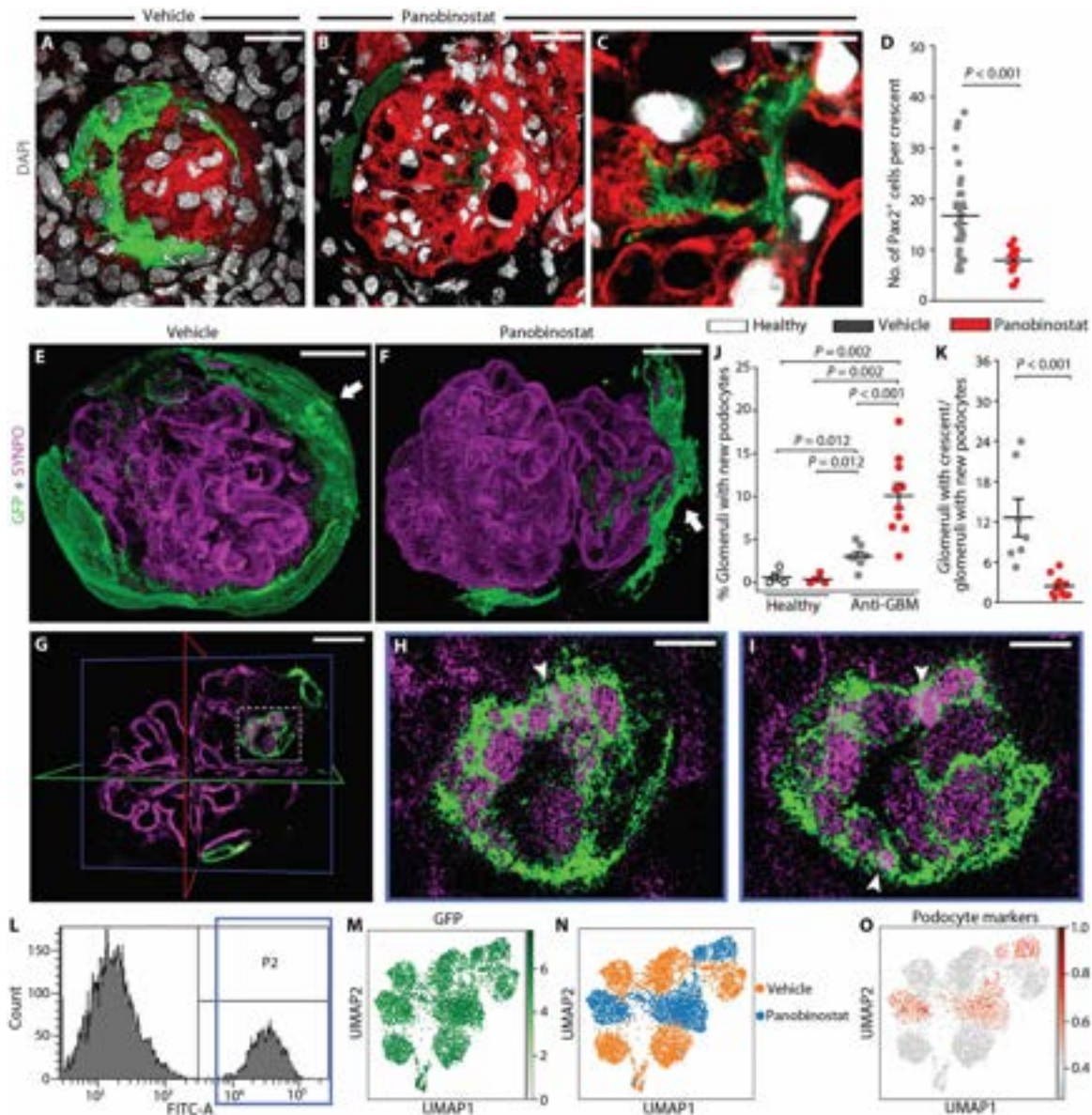
Fig. 4. Panobinostat enhances generation of new podocytes. (**A**) Representative glomerulus in a kidney section from a *Pax2.rtTA;TetO.Cre;R26.mT/mG* mouse with crescentic glomerulonephritis showing a Pax2+ hyperproliferative lesion (green) after treatment with vehicle. Scale bar, 20 μm. (**B**) Representative image of a glomerulus in a kidney section from a *Pax2.rtTA;TetO.Cre;R26.mT/mG* mouse with crescentic glomerulonephritis showing Pax2+-derived cells inside the glomerular tuft after panobinostat treatment. Scale bar, 20 μm. (**C**) Higher magnification of (B) showing foot processes of the Pax2+-derived cell. DAPI (white) was used to counterstain nuclei. Scale bar, 10 μm. (**D**) Dot plot of the 3D analysis of (A) to (C) showing the number of Pax2+ cells within the crescents of kidney sections from vehicle-treated (n = 6) and panobinostat-treated (n = 4) *Pax2.rtTA;TetO.Cre;R26.mT/mG* mice. (**E** to **I**) 3D reconstructions of whole glomeruli using optical tissue clearing of kidney sections from *Pax2.rtTA; TetO.Cre;R26.mT/mG* mice with crescentic glomerulonephritis. The panels show patterns of glomerular lesions based on GFP staining (green, white arrows) and synaptopodin (SYNPO) expression (magenta) in anti-GBM–injected mice treated with vehicle (E) or panobinostat (F). Scale bars, 20 μm. (G) A *z* plane within the glomerulus shown in (F) indicating a newly formed podocyte (green). The position of *x* (green), *y* (red), and *z* (blue) axes is reported. Scale bar, 20 μm. (H and I) Higher magnifications of the boxed area in (G). Different planes along the *z* axis show foot processes of the Pax2+-derived podocyte (green) interdigitating with foot processes of preexisting podocytes (magenta). White arrowheads indicate interdigitation. Scale bars, 5 μm. (**J**) Percentage of glomeruli with new podocytes over total number of glomeruli in vehicle-treated (n = 4) and panobinostat-treated (n = 4) healthy mice and in vehicle-treated (n = 7) and panobinostat-treated (n = 10) mice injected with anti-GBM antibodies. New podocytes were identified as GFP+ cells (green) within the glomerular tuft presenting features of podocyte cells. (**K**) Dot plot showing ratio of glomeruli with crescents to glomeruli with newly formed podocytes in vehicle-treated (n = 7) and panobinostat-treated (n = 10) mice injected with anti-GBM antibodies. (**L**) Gating strategy to isolate Pax2+ cells from renal progenitor cells in the kidneys of *Pax2.rtTA;TetO.Cre;R26.mT/mG* mice (n = 2). The far right peak (P2) containing GFP+ cells was isolated by cell sorting. (**M**) UMAP visualization of GFP expression in Pax2+ cells isolated from the kidneys of *Pax2.rtTA;TetO.Cre;R26.mT/mG* mice (n = 2). (**N**) UMAP projection of Pax2+ cell scRNAseq datasets from vehicle-treated (orange) and panobinostat-treated (blue) *Pax2.rtTA;TetO.Cre;R26.mT/mG* mice. (**O**) UMAP visualization of Pax2+ cell scRNAseq datasets from vehicle- and panobinostat-treated *Pax2.rtTA;TetO.Cre;R26.mT/mG* mice from (N) showing expression of the podocyte markers *Nphs1*, *Nphs2*, *Wt1*, *Map4k2*, *Podxl*, *Pla2g7*, *Mapt*, *Klf14*, and *Ncam1* (orange). In (A) to (C), signals for fluorescent *mT/mG* proteins are GFP (green) and tdTomato (red). In dot plots (D), (J), and (K), bars indicate mean values. Individual scores are shown. Statistical significance was calculated by Mann-Whitney test (D, J, and K).

Fig. 5. Panobinostat improves 3D glomerular structure and slit diaphragm integrity. (**A** to **F**) 3D reconstructions of whole glomeruli using optical tissue clearing of kidney sections from healthy mice (A and B) and *Pax2.rtTA;TetO.Cre;R26.mT/mG* mice with crescentic glomerulonephritis (C to F). Expression of podocin (NPHS2) is indicated with a depth coding profile to preserve z-information. (C and D) Patterns of glomerular lesions (white asterisks) based on NPHS2 expression in vehicle-treated *Pax2.rtTA;TetO.Cre;R26.mT/mG* mice. (E and F) Glomerular structure in panobinostat-treated *Pax2.rtTA;TetO.Cre;R26.mT/mG* mice. Scale bars, 20 μm. (**G**) Percentage of glomeruli with improved slit diaphragm integrity assessed in fluorescently labeled optically cleared kidney tissue from vehicle-treated ($n = 4$) and panobinostat-treated *Pax2. TetO.Cre;R26.mT/mG* mice ($n = 4$). (**H**) Density of slit diaphragms was assessed as a marker of terminal podocyte differentiation using STED superresolution microscopy. The quantification was carried out for five randomly selected areas of each glomerulus in at least five glomeruli per mouse (vehicle treated, $n = 4$ mice; panobinostat treated, $n = 4$ mice). (**I** and **J**) Representative images of podocyte foot processes using STED superresolution microscopy after tissue clearing of kidney sections from vehicle- and panobinostat-treated *Pax2.rtTA;TetO.Cre;R26. mT/mG* mice. NPHS2 is stained in green. Scale bars, 2 μm. In dot plots (G) and (H), bars indicate mean values. Individual scores are shown. Statistical significance in (G) and (H) was calculated by Mann-Whitney test.
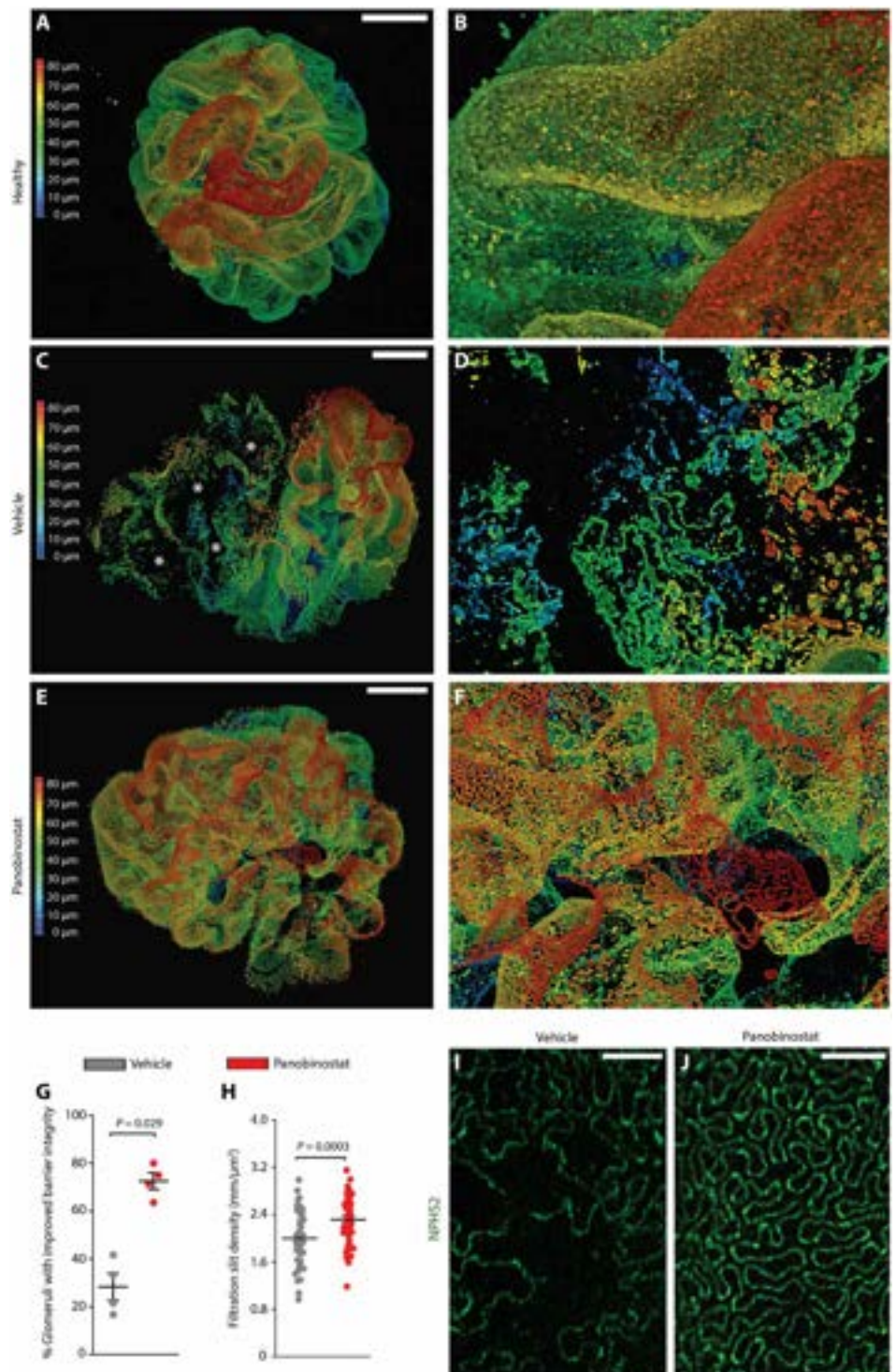
ability to prevent kidney failure after apparent acute phase remission. Toward this aim, we administered the drug to mice on day 4 after the induction of kidney injury, and we followed the mice for 90 days, measuring proteinuria and kidney function at different time points (Fig. 6, A to C, and fig. S9A). Starting treatment with panobinostat at day 4 after injury, i.e., once the peak of proteinuria had passed and crescents were already present, still resulted in a reduction in proteinuria and kidney function recovery (Fig. 6, A to C). The difference was already visible at day 10 after injury, 1 week after the start of treatment (Fig. 6, A to C), and was comparable to the effect observed when the treatment was started at day 1 after injury (fig. S9, B to D). At day 90, mice treated with vehicle achieved a partial remission but with persistent proteinuria, elevated BUN, and reduced GFR. In contrast, mice treated with panobinostat underwent complete remission, exhibiting no proteinuria and normal BUN and GFR (Fig. 6, A to C), and did not develop kidney failure (Fig. 6, A to C).

Analysis of panobinostat-treated mouse kidneys showed a reduction in the percentage of glomeruli with crescents at day 10 after injury ($P = 0.009$) and an almost total disappearance at day 90

($P = 0.008$) (Fig. 6D). This was associated with an increase in the percentage of glomeruli that contained new podocytes at day 10 after injury ($P = 0.009$), and this had further increased at day 90 ($P = 0.016$) (Fig. 6E). At day 90, we also observed an increase in the number of newly generated podocytes per glomerulus in panobinostat-treated mice in comparison not only to vehicle ($P = 0.008$) but also to panobinostat-treated mice at day 10 after injury ($P = 0.008$) (Fig. 6F), suggesting a persistently active repair process over time. Consistently, at day 90,
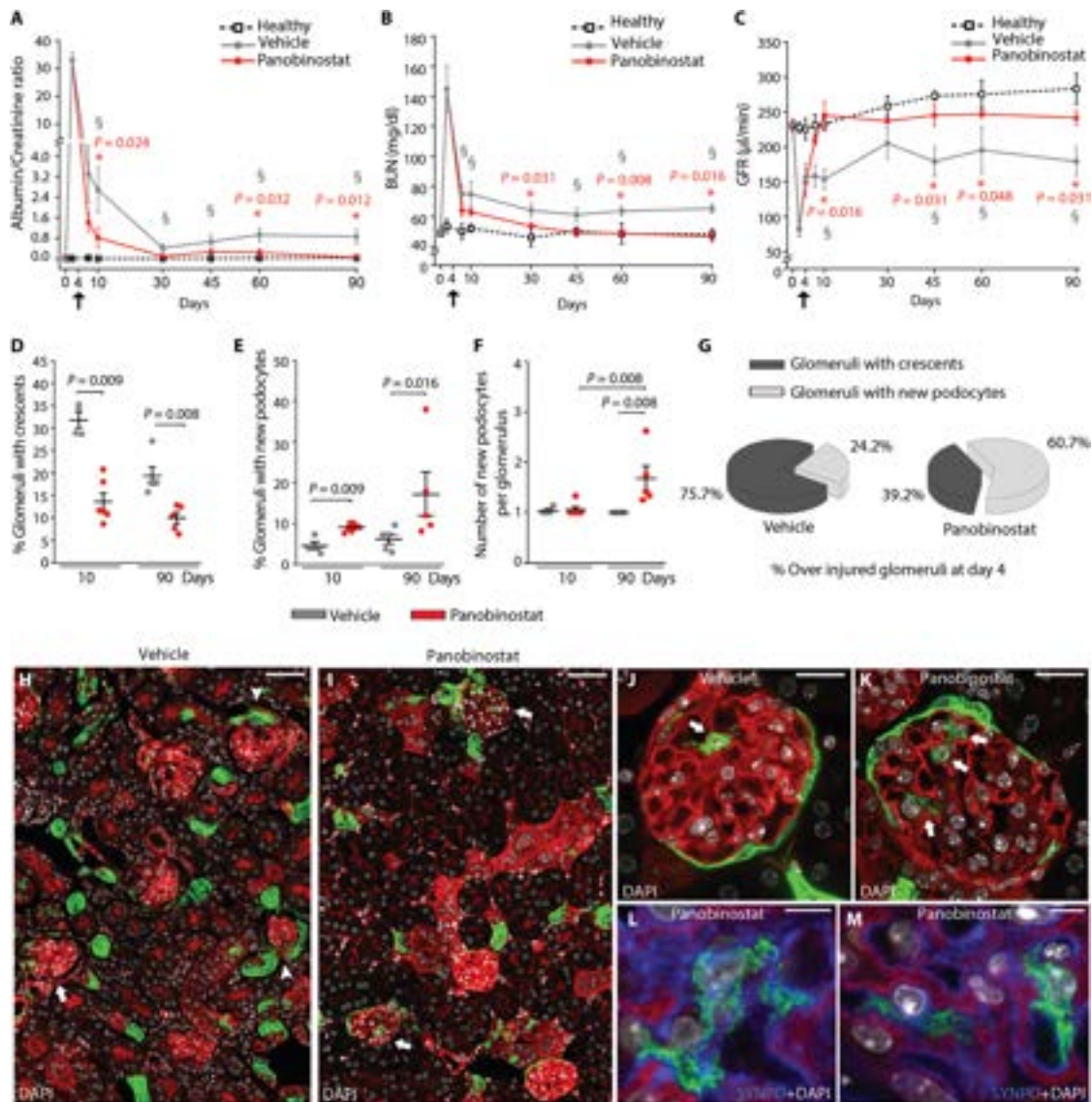
Fig. 6. Panobinostat attenuates crescentic glomerulonephritis and prevents kidney failure in mice. (**A**) Time course of urine albumin/creatinine ratio was determined in healthy mice ($n = 4$) and in mice with crescentic glomerulonephritis treated with vehicle ($n = 9$ at days 4 and 10 and $n = 5$ at days 30, 45, 60, and 90 after injection of anti-GBM serum) or panobinostat ($n = 11$ at days 4 and 10 and $n = 5$ at days 30, 45, 60, and 90 after injection of anti-GBM serum). (§) Significance of vehicle versus healthy mice: day 10, $P = 0.004$; days 30, 45, 60, and 90, $P = 0.016$. (*) Significance of panobinostat versus vehicle. (**B**) Time course of BUN values determined in healthy mice ($n = 4$) and in *Pax2.rtTA;TetO.Cre;R26.mT/mG* mice with crescentic glomerulonephritis treated with vehicle ($n = 9$ at days 4 and 10 and $n = 5$ at days 30, 45, 60, and 90 after injection of anti-GBM serum) or panobinostat ($n = 11$ at days 4 and 10 and $n = 5$ at days 30, 45, 60, and 90 after injection of anti-GBM serum). (§) Significance of vehicle versus healthy mice: days 7 and 10, $P = 0.019$; days 45, 60, and 90, $P = 0.032$. (*) Significance of panobinostat versus vehicle. (**C**) Glomerular filtration rate (GFR) was determined in healthy mice ($n = 4$) and in *Pax2.rtTA;TetO.Cre;R26.mT/mG* mice with crescentic glomerulonephritis treated with vehicle ($n = 5$) or panobinostat ($n = 4$). Black arrows indicate the starting point for drug treatment. Data are means ± SEM. (§) Significance of vehicle versus healthy mice: days 10, 45, and 90, $P = 0.016$; day 60, $P = 0.032$. (*) Significance of panobinostat versus vehicle. (**D**) Percentage of glomeruli with crescents in *Pax2.rtTA;TetO.Cre;R26.mT/mG* mice at day 10 (vehicle, $n = 4$; panobinostat, $n = 6$) and day 90 (vehicle, $n = 5$; panobinostat, $n = 5$) after anti-GBM serum injection. (**E**) Percentage of glomeruli with new podocytes over total number of glomeruli in *Pax2.rtTA;TetO.Cre;R26.mT/mG* mice at day 10 (vehicle, $n = 4$; panobinostat, $n = 6$) and day 90 (vehicle, $n = 5$; panobinostat, $n = 5$) after anti-GBM serum injection. (**F**) Dot plot showing the mean number of Pax2^{+} cells observed within glomeruli in *Pax2.rtTA;TetO.Cre;R26.mT/mG* mice at day 10 (vehicle, $n = 4$; panobinostat, $n = 6$) and day 90 (vehicle, $n = 5$; panobinostat, $n = 5$) after anti-GBM serum injection. (**G**) Percentage of glomeruli with crescents and glomeruli with new podocytes observed in kidney sections from *Pax2.rtTA;TetO.Cre;R26.mT/mG* mice at day 90 (vehicle, $n = 5$; panobinostat, $n = 5$) after anti-GBM serum injection. Percentages were calculated among glomeruli presenting crescents at day 4 after anti-GBM serum injection. (**H** and **I**) Representative images of kidney sections from vehicle-treated (H) or panobinostat-treated (I) *Pax2.rtTA;TetO.Cre;R26.mT/mG* mice sacrificed at day 90. White arrows indicate the presence of Pax2^{+}-derived cells inside the glomerular tuft. White arrowheads indicate the presence of crescents. Scale bars, 50 μm. (**J** and **K**) Representative images of a glomerulus showing Pax2^{+}-derived cells (green) inside the glomerular tuft (white arrows) in vehicle-treated (J) or panobinostat-treated (K) *Pax2.rtTA;TetO.Cre;R26.mT/mG* mice sacrificed at day 90. Scale bars, 20 μm. (**L** and **M**) Higher magnification of (K) showing foot processes and synaptopodin (SYNPO) expression (blue) in the Pax2^{+}-derived cells in kidneys from panobinostat-treated *Pax2.rtTA;TetO.Cre;R26.mT/mG* mice sacrificed at day 90. DAPI (white) was used to counterstain nuclei. Scale bars, 5 μm. In (H) to (M), signals for fluorescent mT/mG proteins are GFP (green) and tdTomato (red). In dot plots (D) to (F), bars indicate mean values. Individual scores are shown. Statistical significance in (A) to (F) was calculated by Mann-Whitney test.

glomeruli with newly generated podocytes corresponded to 60.7% of glomeruli that showed crescents on day 4 (at the start of treatment) in panobinostat-treated mice compared to only 24.3% in vehicle-treated mice (Fig. 6G). Representative images are shown in Fig. 6 (H to M). Together, these results show that panobinostat exerted long-term nephroprotective effects by persistently promoting the production of new podocytes for continued glomerular repair.

Expansion within crescents of a PEC subset expressing CD133 and stratifin is associated with clinical outcome

To identify the PEC subset generating crescents in humans, we obtained PEC cultures from outgrowth of glomeruli from healthy human kidney (*30*) and performed scRNAseq analysis. Clustering of the entire pooled dataset identified seven transcriptionally distinct populations (Fig. 7A), and for each of them, we looked for the 50 genes that characterized the clusters (table S1). By cross-referencing genes that were enriched in these clusters with the published literature, we observed that clusters 4 and 5 were highly enriched in previously reported crescent markers (Fig. 7B) (*8*). In addition, cluster 4 was enriched for genes with roles in cellular pathways intimately linked to crescents, stem cell niches (*6, 31, 32*), and cancer stem cells (*33–35*) such as *EPCAM, CD9, CD24, SFN, LAMC2, CRNDE, HOXB9,* and *CDA* (table S1). To verify the progenitor cell signature of cluster 4, we analyzed the PEC outgrowth dataset together with a previously described renal progenitor cell dataset (Fig. 7, C to E) (*36*). By matching them through the mutual nearest neighbors batch correction algorithm, we obtained a matrix of 7443 cells that showed a high correspondence between some PEC clusters and renal progenitor cells. Louvain clustering revealed a large overlap between the cluster 4 present in the PEC dataset and cluster 2 of the renal progenitor cell/PEC dataset (fig. S10A). Consistently, cluster 2 was enriched for genes with roles in cellular pathways linked to crescents, such as *CD44* and *CD9*, and cancer stem cells, such as *EPCAM* and *SFN* (*32*), as well as the renal progenitor cell markers *CD133* (*PROM1*) and *CD24* (Fig. 7F). Stratifin, encoded by *SFN*, is a cell cycle checkpoint protein involved in stem cell proliferation/differentiation (*37*) that showed selective expression in renal progenitor cells/PECs of cluster 2. We then analyzed stratifin expression in healthy human glomeruli and in the glomeruli of 22 patients with crescents in their kidney biopsies, 13 patients with ANCA-associated vasculitis (AAV) and 9 patients with LN selected following the flow chart shown in fig. S11. Tables S2 and S3 list the clinical characteristics of AAV and LN patients, respectively. Double immunolabeling for CD133 and stratifin in glomeruli of healthy patients confirmed the existence of a subset of CD133^{+} progenitor cells in the Bowman capsule expressing stratifin that represented 15.0 ± 1.5% of the CD133^{+} PEC population (Fig. 7G); in crescents, these stratifin-expressing cells represented 64.3 ± 2.5% of the CD133^{+} PEC population (Fig. 7, H and I). Comparison between patients on the basis of their progression to end-stage kidney disease after 2 years of follow-up (tables S2 and S3) showed that whereas the percentage of glomeruli with crescents, crescent dimension, and percentage of CD133^{+}SFN^{−} cells was similar (Fig. 7, J and K, and tables S2 and S3), the percentage of CD133^{+}stratifin^{+} cells constituting the crescents was lower in the group with a good outcome (*P* < 0.001) (Fig. 7L and tables S2 and S3). In addition, patients with a good prognosis showed a higher percentage of CD133^{−}stratifin^{−} cells in their crescents (*P* < 0.001) (Fig. 7M), which was at least in part related to a higher number of podocytes (*P* < 0.001) (Fig. 7, N to Q).

Although in a small number of patients, these results suggest that crescents mostly result from the amplification of CD133^{+}stratifin^{+} PECs and that the extent of involvement of this cell population may be associated with clinical outcome.

Panobinostat promotes differentiation of human renal progenitor cells into podocytes

The results obtained in human kidney biopsies, suggesting CD133^{+}-SFN^{+} PECs as the cells of origin of crescents, prompted us to verify the effects of panobinostat observed in the mouse model of crescentic glomerulonephritis in human renal progenitor cell primary cultures. Givinostat and ruxolitinib were tested as additional controls. All three drugs reduced metabolic activity of human renal progenitor cells obtained from patient kidney tissue in vitro, with panobinostat being the most effective as assessed by the 3-(4,5-dimethylthiazol-2-yl)-2,5-diphenyltetrazolium bromide (MTT) cell viability test (*P* < 0.001) (Fig. 8A). This reduced metabolic activity was associated with a sharp reduction in the number of cells, i.e., an antiproliferative effect (*P* = 0.008) (Fig. 8B). Panobinostat and givinostat also reduced the percentage of live cells as detected by the annexin V/propidium iodide assay (*P* = 0.002) (Fig. 8C and fig. S12A). However, cell cycle analysis by flow cytometry also highlighted a doubling of the percentage of renal progenitor cells in the G_2-M phase after panobinostat, givinostat, or ruxolitinib treatment, suggesting that all three drugs promoted cell cycle arrest (Fig. 8D and fig. S12B). Together, drugs that inhibit hematopoietic progenitor cell proliferation also inhibited the proliferation of renal progenitor cells. We then evaluated the capacity of these drugs to modulate renal progenitor cell differentiation into podocytes. We used all-trans retinoic acid (ATRA) as a positive control given its well-defined effect as an inducer of renal progenitor cell differentiation into podocytes (*10, 38*). Panobinostat was much more efficient than ATRA (*39*) in promoting renal progenitor cell differentiation into podocytes, as demonstrated by the change in cell morphology shown by tubulin staining and superresolution microscopy (Fig. 8E), and the high expression of *NPHS2* and *NPHS1* mRNAs (Fig. 8, F and G) as well as proteins (Fig. 8, H and I). Givinostat only increased *NPHS1* expression, with *NPHS2* expression not detectable, suggesting a limited effect on progenitor cell differentiation (Fig. 8, F to I). Ruxolitinib did not induce *NPHS2* or *NPHS1* expression (Fig. 8, F to I).

Comparison of the single-cell transcriptome of control and panobinostat-treated PEC cultures obtained from outgrowth of glomeruli from healthy human kidney (Fig. 8J) confirmed that panobinostat induced up-regulation of podocyte-specific markers including *NPHS1, NPHS2, MAFB, MAPT, KFL14, KFL15, PLA2G7, PTPRO,* and *SYNPO* in different PEC subsets including stratifin-expressing renal progenitor cells (Fig. 8, K to M). Panobinostat treatment also down-regulated expression of stratifin as well as genes of the Notch and β-catenin pathways (Fig. 8N), which are involved in promoting renal progenitor cell proliferation and inhibiting their differentiation into podocytes, respectively. Together, the data show that panobinostat blocks mouse and human podocyte progenitor cell proliferation and induces differentiation of these cells into podocytes.

DISCUSSION

Crescent formation in the kidney compromises glomerular filtration and urine outflow independent of the upstream pathomechanisms of necrosis. Treatments specifically targeting the causative uncontrolled

Fig. 7. Expansion in crescents of a PEC subset expressing CD133 and stratifin is associated with patient outcomes. (**A**) UMAP of an scRNAseq dataset from a human PEC culture, showing different clusters. (**B**) UMAP visualization of expression of markers of renal progenitor cells (*CD24* and *PROM1*) and crescents (*CD44* and *CD9*). Color intensity indicates level of expression. (**C** and **D**) UMAP projection of integrated renal progenitor cell (blue) and PEC (orange) datasets showing samples (C) and clusters (D). (**E**) Heatmap representing the expression of the top 12 markers of each cluster shown in (D). (**F**) UMAP visualization of stem cell (*PROM1* and *CD24*) and cancer stem cell marker (*CD9*, *EPCAM*, and *SFN*) expression. Color bar indicates log$_2$-normalized expression. (**G** to **I**) Representative images showing CD133 expression (red) and stratifin (SFN) expression (green) and localization in kidney biopsies from a healthy individual (G) and two patients diagnosed with ANCA-associated vasculitis (AAV) that progressed (H) or did not progress (I) to end-stage kidney disease (ESKD). White arrows indicate regions with CD133 and SFN co-expression in healthy tissue. DAPI (white) was used to counterstain nuclei. Scale bars, 25 μm. (**J**) Graph representing the number of cells per crescent in patients with AAV progressing (gray dots, $n = 10$) or not progressing (blue dots, $n = 12$) to ESKD. (**K** to **M**) Graphs show the percentage of CD133$^+$SFN$^+$ cells (K), CD133$^+$SFN$^-$ cells (L), and CD133$^-$SFN$^-$ cells (M) over the total number of cells within the crescent in kidney biopsies from patients with AAV that progressed ($n = 10$, gray dots) or did not progress ($n = 12$, blue dots) to ESKD. (**N** and **O**) Representative images showing CD133 expression (red) and NPHS2 (podocin; cyan) expression and localization in kidney biopsy tissue obtained from patients with AAV that progressed (N) or did not progress (O) to ESKD. White arrows indicate CD133$^-$NPHS2$^+$ cells in a crescent. Scale bars, 25 μm. (**P**) Magnification of (O). White arrow indicates CD133$^-$NPHS2$^+$ cells in a crescent. DAPI (white) was used to counterstain nuclei. Scale bar, 10 μm. (**Q**) Quantification of the percentage of CD133$^-$NPHS2$^+$ cells over the total number of cells within the crescent in patients with AAV that progressed ($n = 10$) or did not progress ($n = 12$) to ESKD. In dot plots (J) to (M) and (Q), bars indicate mean values. Individual scores are shown. Statistical significance was calculated by Mann-Whitney test (J to M).
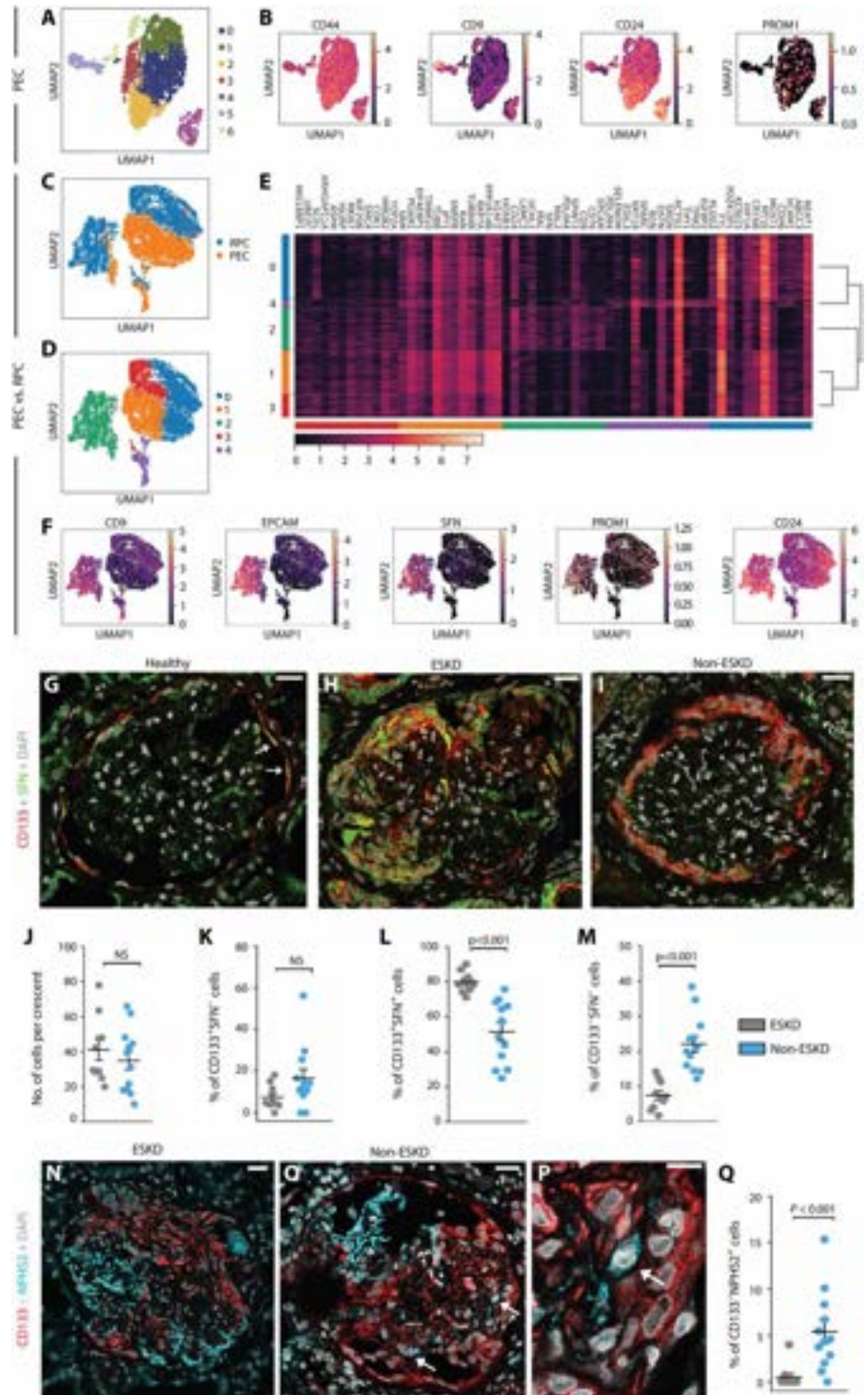

hyperplasia of PECs are not available. In this study, we show that (i) crescents form via clonal proliferation of single cells from a particular immature subset of PECs in the Bowman capsule; (ii) panobinostat, an inhibitor of clonal proliferation used for treatment of clonal hematopoietic diseases, successfully reduced proteinuria and boosted kidney function recovery, in a mouse model of crescentic glomerulonephritis; and (iii) the beneficial effect of panobinostat was associated with its capacity to turn the uncontrolled hyperplasia of immature renal progenitor cells into controlled differentiation into new podocytes, thereby restoring the injured glomerular filtration barrier.

Crescents have been thought to represent an overexuberant epithelial healing response of the PECs lining the Bowman capsule

in response to rupture of the GBM during capillary loop necrosis (*1*, *2*). Using lineage tracing analysis of Pax2$^+$ podocyte progenitors, clonal analysis with the Confetti reporter, and scRNAseq, we show that a distinct PEC subpopulation forms the crescent. This reflects heterogeneity among PECs in terms of both differentiation potential and proliferative capacity (*13*, *40*). We identified the subset of PECs that form the crescents by clonal expansion according to an

Melica *et al.*, *Sci. Transl. Med.* **14**, eabg3277 (2022)   10 August 2022

10 of 17

Fig. 8. Panobinostat inhibits proliferation and promotes differentiation of human renal progenitor cells. (**A**) MTT assay of primary human renal progenitor cells treated with panobinostat, givinostat, or ruxolitinib for 48 hours to measure cell proliferation and survival. Data were obtained from three different primary cultures in three independent experiments. Each dot represents the mean of technical triplicates. (**B**) Number of renal progenitor cells after 48 hours of treatment with panobinostat, givinostat, or ruxolitinib. Data were obtained from three different primary cultures in two independent experiments. Each dot represents the mean of technical triplicates. (**C**) Quantification of live cells using annexin V/propidium iodide fluorescence-activated cell sorting (FACS) staining for assessment of apoptosis induction after treatment with panobinostat, givinostat, or ruxolitinib for 48 hours. Data were obtained from three different primary cultures in three independent experiments. Each dot represents the mean of technical triplicates. (**D**) Distribution of renal progenitor cells in different cell cycle phases assessed by flow cytometry after panobinostat, givinostat, or ruxolitinib treatment for 48 hours. Data were obtained from three different primary cultures in two independent experiments. (**E**) Representative STED images showing cytoskeleton changes associated with differentiation into podocytes based on tubulin expression in primary human renal progenitor cells after treatment with panobinostat, givinostat, or ruxolitinib for 48 hours. Untreated cells and cells treated with all-trans retinoic acid (ATRA), which induces differentiation into podocytes, were used as a negative and positive control, respectively. One representative experiment of three independent experiments is shown. DAPI (white) was used to counterstain nuclei. Scale bars, 20 μm. (**F** and **G**) Expression of the podocyte-specific markers NPHS1 (nephrin) and NPHS2 (podocin) in primary human renal progenitor cells after treatment with ATRA, panobinostat, givinostat, or ruxolitinib for 48 hours. mRNA expression of NPHS2 (F) and NPHS1 (G) was determined by real-time reverse transcription polymerase chain reaction (RT-PCR) and reported as fold increase over untreated cells. Data were obtained from three different primary cultures in three independent experiments. Each dot represents the mean of technical triplicates. (**H** and **I**) Representative confocal microscopy images showing expression of the podocyte markers NPHS2 and NPHS1 (red) after treatment with panobinostat, givinostat, or ruxolitinib for 48 hours. Untreated and ATRA-treated cells were used as negative and positive control, respectively. One representative experiment of three independent experiments is shown. DAPI (white) was used to counterstain nuclei. Scale bars, 25 μm. (**J**) UMAP of human PEC culture scRNAseq datasets before (orange, control) or after treatment with panobinostat (blue). (**K**) UMAP visualization of expression of the podocyte markers NPHS2 and NPHS1 (red) in human PEC culture scRNAseq datasets before or after treatment with panobinostat. (**L**) UMAP of human PEC culture scRNAseq datasets before or after treatment with panobinostat showing clustering. (**M**) UMAP visualization of stratifin (SFN; red) expression in human PEC culture scRNAseq datasets before or after treatment with panobinostat. (**N**) Dot plot showing the expression of genes related to crescent formation or in the NOTCH or WNT pathways that were affected by panobinostat treatment of human PEC cultures. In dot plots (A) to (C), (F), and (G), bars indicate mean values. Individual scores are shown. Statistical significance was calculated by Mann-Whitney test.

Melica *et al.*, *Sci. Transl. Med.* **14**, eabg3277 (2022)   10 August 2022

11 of 17
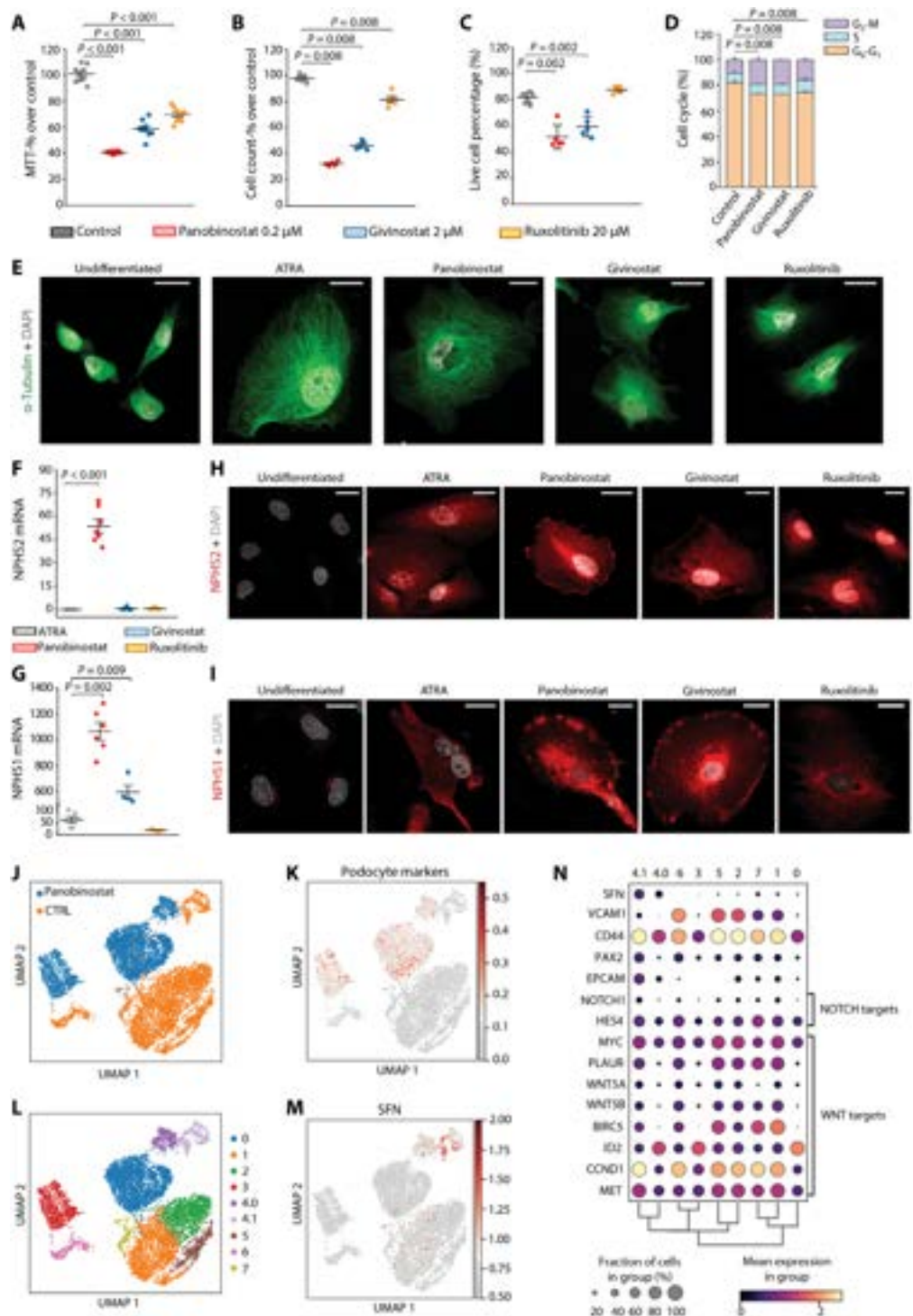
expression pattern similar to stem cells of other organs and tissues, including hematopoietic stem cells. This further underlines the similarities between the stem cells of the kidney and of the bone marrow, as previously suggested (40, 41). The bone marrow stem cell niche of hematopoietic stem cells includes endothelial cells producing CXCL12, which keeps hematopoietic stem cells largely in a quiescent state (13). The glomerulus where renal progenitor cells reside among the PECs along the inner aspect of the Bowman capsule shows similarities with the bone marrow stem cell niche (5). Under healthy conditions, podocytes produce high amounts of CXCL12 to keep renal progenitor cells among the PECs quiescent and undifferentiated (5). Other similarities relate to the expression of CD44 (7) and VCAM1 (42) by renal progenitor cells and their role in renal progenitor cell activation. In addition, the local presence of high amounts of vascular endothelial growth factor (VEGF) (43) and transforming growth factor–β (TGF-β) (12) also contributes to renal progenitor cell quiescence and survival, like in the bone marrow stem cell niche (44). Crescents develop from clonal proliferation of an immature PEC subset, a podocyte progenitor cell that expands but without differentiating into podocytes, which is similar to other stem cell disorders of the bone marrow (14, 15), gut (45, 46), and skin (47).

We recently reported that injury of kidney tubules stimulates progenitor cells scattered within kidney tubules to undergo hyperplasia and form papillary adenomas and carcinomas (36). Tubule adenomas may be the tubular equivalent of glomerular crescents. In the case of crescents, stimuli inducing PEC proliferation likely include mitogenic serum factors reaching the Bowman space upon capillary loop necrosis and GBM rupture (48). Even if all PECs are similarly exposed to this mitogenic micromilieu, a particular PEC subset with phenotypic and functional features of progenitor cells has a higher capacity to proliferate consistent with its stem cell features, thus becoming the cell of origin for clonal crescents. The crescent-forming PEC subset is characterized by expression of stratifin, also known as 14-3-3σ. The 14-3-3 proteins are 28- to 33-kDa polypeptides found in all eukaryotic organisms (49). Seven members (b, c, e, g, s, h/t, and f) are found in mammals (50). Through binding to at least 200 proteins including enzymes, transcription factors, cytoskeletal proteins, signaling molecules, apoptosis factors, and tumor suppressors (50), 14-3-3 proteins are pivotal drivers of proliferation and differentiation (50) and essential regulators of stem cell function (51–53) and cancer development (32, 54) in multiple organs and tissues. For example, 14-3-3 proteins interfere with the adaptor protein LNK, a critical inhibitor of JAK2, thereby limiting hematopoietic stem and progenitor cell self-renewal (52). LNK deficiency promotes myeloproliferative neoplasm development in mice (55), and LNK loss-of-function mutations are found in human myeloproliferative disorders (56), suggesting that 14-3-3 proteins are crucial players in these diseases (52). Expression of the 14-3-3 protein stratifin determines the choice between proliferation and differentiation in embryonic stem cells (51). In particular, it induces phosphatidylinositol 3-kinase (PI3K)/Akt activation and triggers dissociation from the adenomatous polyposis coli/axin/glycogen synthase kinase-3b (GSK-3b) complex of β-catenin, which translocates into the nucleus to drive the transcription of mitogenic genes (51). β-Catenin induces PEC proliferation, whereas its deletion promotes PEC differentiation into podocytes (57). In addition, retinoic acid, a crucial driver of progenitor cell differentiation into podocytes (39), selectively suppresses stratifin (51). Last, stratifin[+] renal progenitor cells show low expression of VCAM1. Like hematopoietic cells (58), VCAM1 expression characterizes immature renal progenitor cells that exhibit stem cell potential and are quiescent in the glomerular niche (42). Once VCAM1^{+} renal progenitor cells are committed to podocyte differentiation, they first start to express podocalyxin (42) and then down-regulate VCAM1 before up-regulating podocyte markers and differentiating into podocytes (42). The results of this study suggest that stratifin expression characterizes a VCAM low renal progenitor cell subset functionally committed to proliferate that undergoes clonal expansion (fig. S13). Stratifin[+] renal progenitor cells are characterized by expression of CD44 (59) and CD9 (8), crucial drivers of crescent formation (8, 59). Clonal amplification of this subset promotes crescent formation, as confirmed by the association between the percentage of stratifin-expressing PECs within crescents and a poor outcome in patients with crescentic glomerulonephritis.

Patients with crescentic glomerulonephritis have a high risk of progressing toward end-stage kidney disease, despite therapy (1, 3). Current treatments target upstream autoimmune and inflammatory pathways but do not directly target crescent formation itself (3), although cyclophosphamide that is used for some of these diseases elicits antiproliferative effects not only on immune cells but also on PECs (1). These results provided the rationale for the evaluation of drugs already in use for disorders of clonal stem cell hyperplasia, such as myeloma or primary myelofibrosis (18, 19, 60, 61), for treating crescentic glomerulonephritis. Three drugs showed anti-inflammatory and immunosuppressive effects and reduced viability and proliferation of renal progenitor cells, suggesting common mechanisms mediating clonal amplification in stem cell disorders across different organs, including the kidney. However, when administered to a mouse model of crescentic glomerulonephritis, only panobinostat promoted a reduction in crescent formation and proteinuria as well as kidney function recovery, an effect that was consistent with its capacity to promote differentiation into podocytes of a PEC subset with phenotypic and functional features of progenitor cells. Consistently, this reduction in crescent number was associated with down-regulation of stratifin as well as β-catenin target genes in stratifin-expressing human PECs and with their shift from crescent formation to generation of new podocytes in vivo. These results suggest that inhibition of crescent formation alone cannot efficiently treat crescentic glomerulonephritis. By contrast, drug-induced differentiation of progenitor cells into podocytes can solve two problems: hyperplasia of the immature PECs and repair of the filtration barrier. Delayed treatment with panobinostat, which was administered after the peak of proteinuria and crescent formation, still induced a reduction in proteinuria and amelioration of kidney failure, an effect that was associated with continued generation of new podocytes and crescent regression over time.

There are some limitations to our study. First, the number of biopsies from patients with crescentic glomerulonephritis that were analyzed was small, owing to the rarity of this disease (1). Further studies are needed to confirm the association between CD133^{+}stratifin^{+} PECs in crescents and the risk of progression to end-stage kidney disease. Second, crescentic glomerulonephritis in humans may involve other mechanisms in addition to those targeted in the anti-GBM mouse model used in this study (62). However, studies in patients with different types of myeloproliferative disorders and lymphomas suggest that panobinostat exerts wide immunosuppressive effects that could also be useful for the treatment of crescentic glomerulonephritis (17, 18, 63).

Together, these results offer mechanistic insights into crescent formation suggesting that these lesions are caused by clonal proliferation of single immature PECs and by a lack of their differentiation toward a fully differentiated podocyte phenotype upon severe glomerular injury. Analogous to other disorders caused by dysregulation of the stem cell response, development of these lesions can be interrupted by using drugs that have already been developed and successfully applied to block abnormal clonal stem cell growth in other organs and tissues.

MATERIALS AND METHODS

Study design
The purpose of this study was to examine the contribution of renal progenitor cells among the PEC population to the generation of crescents and to identify the mechanism involved in crescent formation. These objectives were addressed by (i) evaluating renal progenitor cells as the cell of origin of crescents in transgenic mouse models and evaluating crescent clonality, (ii) analyzing the effect of drugs currently used in hematological stem cell disorders on crescentic glomerulonephritis outcome in mouse models, (iii) identifying the crescent-forming human PEC subset by scRNAseq and immunofluorescence analysis on human biopsies from patients with crescentic glomerulonephritis, and (iv) evaluating the mechanisms of panobinostat effects on human renal progenitor cells.

Mice were randomly assigned to experimental and control groups, but investigators were not blinded. Sample size was calculated on the basis of the primary endpoint rate of crescent formation and other assumptions based on preliminary experiments. No data were excluded from studies in this manuscript. Pathology analysis was performed in a blinded fashion. All procedures were performed in accordance with institutional protocols approved by the Institutional Review Board and by the Italian Ministry of Health and performed in accordance with institutional, regional, and state guidelines and with adherence to the National Institutes of Health *Guide for the Care and Use of Laboratory Animals*.

A total of 22 native kidney biopsies of patients (Caucasian ethnicity) with AAV (9 women and 4 men; mean age, 47.5 ± 20.7 years; table S2) and with LN (8 females and 1 male; mean age, 33.5 ± 13.3 years; table S3) were selected for the analysis and retrospectively reviewed in agreement with the Ethical Committee on human experimentation of the Meyer Children University Hospital and of the Careggi University Hospital, Florence, Italy. As controls, normal kidney fragments were obtained from three patients who underwent nephrectomy for localized renal tumors (one woman and two men; mean age, 64.67 ± 8.45 years). These kidney fragments were obtained from the pole opposite to the tumor in agreement with the Ethical Committee on human experimentation of the Careggi University Hospital.

Human kidney biopsies
All biopsies were cut into multiple sections and stained with Jones methenamine silver, PAS, hematoxylin and eosin, and trichrome for clinical purposes. The cohort size was limited by the availability of both clinical data and representative kidney biopsy material; therefore, sample size calculation was not applicable. Initial (time of biopsy) and 2 years of follow-up clinical data were recorded (tables S2 and S3), and the outcome was assigned on the basis of the estimated GFR at 2 years (eGFR < 15 ml/min per 1.73 m^2, end-stage kidney disease; eGFR > 15 ml/min per 1.73 m^2, non–end-stage kidney disease).

Animal studies
The *Pax2.rtTA;TetO.Cre;R26.Confetti* mice or *Pax2.rtTA;TetO.Cre;R26.mT/mG* or *Pax8.rtTA;TetO.Cre;R26.FUCCI2aR* mice were developed on a full C57Bl/6 background by crossing the *Pax2.rtTA* mouse (6, 11) (a gift from B. Schäfer, Department of Oncology and Children's Research Center, University Children's Hospital, Zurich, Switzerland) or the *Pax8.rtTA* mouse [*B6.Cg-Tg(Pax8-rtTA2S*M2)1Koes/J*, IMSR catalog no. JAX:007176, RRID:IMSR_JAX:007176] with the TetO.Cre strain *B6.Cg-Tg(TetO-Cre)1Jaw/J* [International mouse strain resource (IMSR) catalog no. JAX:006234, Research resource identifier (RRID):IMSR_JAX:006234] purchased from The Jackson Laboratory (Bar Harbor, ME, USA). Double transgenic mice were then crossed either with the Confetti strain *Gt(ROSA)26Sor^{tm1(CAG-Brainbow2.1)Cle}/J* [IMSR catalog no. JAX:017492, RRID:IMSR_JAX:017492], with the mT/mG strain *B6.129(Cg)-Gt(ROSA)26Sor^{tm4(ACTB-tdTomato,-EGFP)Luo}/J* (IMSR catalog no. JAX:007676, RRID:IMSR_JAX:007676) (both from The Jackson Laboratory), or with FUCCI2aR strain *B6;129-Gt(ROSA)26Sor^{tm1(Fucci2aR)Jkn/Jkn}Rbrc* (IMSR catalog no. RBRC06511, RRID:IMSR_RBRC06511) to obtain a triple transgenic inducible mouse model.

Mice were genotyped as reported in supplementary methods, and triple homozygous mice were used. Transgene recombination was induced at 6 weeks of age by administration of 4 mg/ml (*Pax2.rtTA;TetO.Cre;R26.Confetti*) or 2 mg/ml (*Pax2.rtTA;TetO.Cre;R26.mT/mG* and *Pax8.rtTA;TetO.Cre;R26.FUCCI2aR*) of doxycycline hyclate (Sigma-Aldrich, St. Louis, MO, USA) in drinking water supplemented with 2.5% sucrose (Sigma-Aldrich) for 10 days, followed by a 7-day washout. Uninduced animals showed no leakage or nonspecific transgene expression.

The Confetti reporter, upon induction, allowed the stochastic labeling of the cells by permanent recombination of a single color-encoding gene [red (RFP), yellow (YFP), green (GFP), or cyan fluorescent proteins (CFP)], with GFP cells occurring at lower frequency than other colors and being extremely rare (13, 64, 65). In homozygous animals, the combination of two color-encoding genes located on the two homologous alleles is possible (red/yellow, red/cyan, red/green, yellow/yellow, yellow/cyan, etc.), and the resulting outcomes are shown in Fig. 2I. This technique allowed us to evaluate the clonal composition of the lesions, because all labeled cells will generate same color labeled cells after proliferation (11).

In the mT/mG reporter, after doxycycline administration, membrane-targeted GFP genetically labels Pax2-expressing cells in green, whereas all the other kidney cells are labeled in red by the membrane-targeted tdTomato fluorescent protein. Anti-GBM serum was injected in *Pax2.rtTA;TetO.Cre;R26.Confetti*, *Pax2.rtTA;TetO.Cre;R26.mT/mG*, or *Pax8.rtTA;TetO.Cre;R26.FUCCI2aR* male mice by an intravenous injection of 150 μl of anti-GBM serum (PTX-001 sheep anti-rat GBM serum, Probetex Inc., San Antonio, TX). In drug administration experiments, mice were randomly assigned to various groups after anti-GBM injection: (i) vehicle (distilled water), (ii) panobinostat (15 mg/kg) (LBH-589, MedChemExpress, Solluntuna, Sweden), (iii) givinostat (10 mg/kg) (ITF2357, Selleckchem, Munich, Germany), and (iv) ruxolitinib (60 mg/kg) (INCB18424, MedChemExpress). Animals were sacrificed 1, 3, 7, 10, or 90 days after anti-GBM serum injection. Healthy male mice were sacrificed at the same time point and used as control. The number of mice used, numbers of replicates, and statistical values (where applicable) are provided in the figure legends.

In *Pax8.rtTA;TetO.Cre;R26.FUCCI2aR* mice, after doxycycline administration, Pax8-expressing cells are labeled with the FUCCI2aR

Melica et al., Sci. Transl. Med. 14, eabg3277 (2022)   10 August 2022

13 of 17

reporter, which consists of a bicistronic Cre-activable reporter of two fluorescent proteins whose expression alternates based on cell cycle phase as follows: mCherry-hCdt1 (30/120) (red), expressed by nuclei of cells in G_1 phase, and mVenus-hGem (1/110) (green), expressed by nuclei of cells in S-G_2-M. Cells can also appear as yellow at the G_1-S boundary (*11*, *66*).

Optical tissue clearing and confocal 3D reconstruction

For the 3D reconstruction of the whole glomeruli and for quantification of filtration slit density, optical clearing of the kidneys was performed. Briefly, kidneys were dissected and immediately incubated at 4°C in hydrogel solution [2% (v/v) acrylamide, 0.025% (v/v) bisacrylamide, 0.25% (w/v) VA-044 initiator, 4% paraformaldehyde, and 1× phosphate-buffered saline (PBS)] for 1 day. The gel was polymerized at 37°C for 3 hours, and the presence of oxygen was minimized by filling tubes to the top with hydrogel solution. Samples were removed from the hydrogel solution, immersed in clearing solution (200 mM boric acid, 4% SDS, pH 8.5), and incubated at 50°C for 1 day. Kidneys were cut in 300-µm-thick slices using a vibratome and incubated at 50°C for 4 days with clearing solution changed every day. Before immunolabeling, samples were incubated in PBST (0.1% Triton X-100 in 1× PBS) for 1 day. During immunolabeling, PBST was used as diluent in all steps. Samples were incubated in primary antibody for 24 hours at 37°C and then washed in PBST for 4 hours at 37°C followed by secondary antibody incubation for 24 hours at 37°C and washed for 4 hours at 37°C before mounting. The following primary antibodies were used: anti-NPHS2 (Sigma-Aldrich, catalog no. P0372, RRID:AB_261982), anti-GFP (Abcam, catalog no. ab6556, RRID:AB_305564), and anti-synaptopodin (Progen Biotechnik, Heidelberg, Germany, catalog no. 65194, clone G1D4, RRID:AB_2909601). Secondary antibodies were obtained from Molecular Probes (Thermo Fisher Scientific). Samples were mounted in 80.2% fructose with 0.5% (v/v) 1-thioglycerol.

To generate 3D reconstructions of glomeruli, Z-series stacks were obtained from 300-µm kidney slices. Images were collected at 1-µm intervals by using a Leica SP8 confocal microscope and deconvolved with Huygens Professional software (Scientific Volume Imaging B.V., Hilversum, The Netherlands). We used image processing software from Leica Microsystems "Leica Application Suite X" for 3D reconstruction.

STED microscopy and slit diaphragm density quantification

STED *xyz* images (i.e., z stacks acquired along three directions: *x*, *y*, and *z* axes) were acquired by using an SP8 STED 3× confocal microscope (Leica Microsystems). Alexa Fluor tetramethyl rhodamine isothiocyanate (TRITC) secondary antibody was excited with a 555-nm tuned white light laser, and emission was collected from 565 to 605 nm. A 660-nm pulsed depletion laser was used with a gating between 0.7 and 6 ns. Images were acquired with Leica HC PL APO CS2 100×/1.40 oil STED White objective.

Collected images were deconvolved with Huygens Professional software version 18.04. For the quantification of filtration slit coverage, z stacks of NPHS2 signal were acquired (at least 5 µm thick). All the images of each z stack were merged, and the foot process length and the area of the field were manually dissected and measured with ImageJ. The total length of the foot processes was divided by the total area of interest. The analysis was carried out in eight randomly selected mice ($n = 4$ vehicle and $n = 4$ panobinostat-treated mice); five randomly selected areas for each glomerulus of at least five

glomeruli per mouse were evaluated. For STED acquisition on progenitor cell culture, the following antibodies were used: anti–α-tubulin (Sigma-Aldrich, catalog no. T6074, RRID:AB_477582) and goat anti-mouse IgG1 546 secondary antibody (Thermo Fisher Scientific).

Clone frequency analysis

Single-cell clones and clones with two or more cells were counted within the inner circumference of Bowman capsule in 3D reconstructed glomeruli of healthy and crescentic glomerulonephritis *Pax2.rtTA;TetO.Cre;R26.Confetti* mice at 7 days. For each clone size, clone frequency analysis shown in Fig. 2F was assessed by calculating the relative frequency $F_{(i)}$ as follows:

$$F_{(i)} = \text{Clone frequency (\%)} = \frac{\text{n° of clones of } n \text{ cells}}{\text{Total n° of clones}} \times 100$$

where $1 \leq n \leq 24$ in *Pax2.rtTA;TetO.Cre;R26.Confetti* mice because this is the maximum clone size observed.

To simplify the large dataset, the clones that contain more than five cells were grouped in class intervals and then cumulative frequency $F_{(k)}$ was calculated for each group using the following formula:

$$F_{(k)} = \sum_{i \in S} f_{(i)}$$

where cumulative frequency $F_{(k)}$ is the sum of overall relative frequency $f_{(i)}$ in the set S (where S is the class interval).

Reconstructed glomeruli were analyzed in a blinded manner (78 glomeruli from nine healthy mice; 32 glomeruli from six crescentic glomerulonephritis mice). Clone size was established by counting the nuclei counterstained with 4′,6-diamidino-2-phenylindole (DAPI).

Single-cell RNA sequencing

scRNAseq was performed on human PEC derived from whole glomeruli culture prepared as previously described (*30*), in agreement with the Ethical Committee on human experimentation of the Azienda Ospedaliero-Universitaria Careggi, Florence, Italy. Briefly, human kidney fragments were minced and glomeruli were isolated by standard sieving technique through graded mesh screens (60, 80, and 150 mesh). The glomerular suspension was collected, washed, and plated on fibronectin-coated dishes. After 4 to 5 days of culture, isolated glomeruli adhered to the plate, resulting in cellular outgrowth. Glomeruli were detached, and adherent cells were characterized for CD133 and CD24 expression at passage 1. Adherent cells were harvested and filtered using the Flowmi Tip strainer (Miltenyi Biotec) to remove clumps and debris, followed by viability assessment with trypan blue (Sigma-Aldrich) staining. The single-cell suspension with 98% viability was run on a 10× Chromium Single Cell instrument (10x Genomics, Pleasanton, CA) following the manufacturer's instructions, as previously described (*8*, *56*, *67*). The 3′ gene expression libraries were constructed as previously described (*8*, *56*, *67*) and were sequenced on Illumina NextSeq550 (Illumina Inc., San Diego, CA, RRID:SCR_020138).

For scRNAseq of sorted Pax2$^+$ cells, kidneys of healthy *Pax2.rtTA;TetO.Cre;R26.mT/mG* mouse ($n = 2$) were transferred into Endothelial basal medium containing 1% (v/v) penicillin-streptomycin solution. The kidney cortex was minced into small fragments, incubated

for 30 min at 37°C with collagenase type IV (1 mg/ml), and then gently pressed and sieved through a 70-μm mesh cell strainer. Strainer was repeatedly rinsed with cold Dulbecco's phosphate-buffered saline, and the filtrate was collected, washed, and resuspended in RPMI 1640 medium (Sigma-Aldrich) supplemented with 20% fetal bovine serum (FBS) (HyClone, GE Healthcare Life Sciences, Logan, UT, USA) and 1% penicillin-streptomycin solution. Glomeruli were cultured at 37°C in a humidified atmosphere containing 95% air–5% CO_2, and after 5 days, glomerular cell outgrowths were trypsinized and cells were resuspended in D-PBS and sorted for endogenous expression of GFP using BD FACSAria III (Becton Dickinson, Franklin Lakes, NJ, USA, RRID:SCR_016695). After sorting, cells were plated in six-well dishes at a density of 80,000 cells per well in RPMI 1640 supplemented with 20% FBS. After 16 hours of starvation, cells were stimulated for 48 hours with 0.2 μM panobinostat or dimethyl sulfoxide (Sigma-Aldrich) in Dulbecco's modified Eagle's medium–F12 medium (D2906, Sigma-Aldrich) containing 10% FBS (HyClone, GE Healthcare Life Sciences). For scRNAseq, after 48-hour stimuli, cells were harvested and processed as previously described for the run on the 10× Chromium Single Cell instrument (10x Genomics) and the subsequent sequencing on Illumina NextSeq550 (Illumina Inc.).

For scRNAseq analysis on *Pax2.rtTA;TetO.Cre;R26.Confetti* mice (Fig. 3, I to M, and figs. S2 to S4), animals were injected with anti-GBM serum and treated with vehicle (*n* = 2), panobinostat (*n* = 2), givinostat (*n* = 2), or ruxolitinib (*n* = 2) starting from day 1 after injury and sacrificed at day 7. Kidneys were minced into 1-mm pieces with a razor blade and incubated at 37°C in enzyme dissociation buffer containing Liberase (250 U/ml) (Roche) and deoxyribonuclease I (40 U/ml) (Sigma-Aldrich) for 10 min, followed by mechanical dissociation using a gentleMACS tissue dissociator (Miltenyi Biotec). The reaction was stopped by adding 10% FBS, and then the suspension was passed through a 40-μm cell strainer. The dissociated cells were then incubated with erythrocyte lysis buffer (0.8% NH_4Cl). We then proceeded to remove the dead cells using the Dead Cell Removal Kit (Miltenyi Biotec) according to the manufacturer's instruction. Cells were then filtered using the Flowmi Tip strainer and run on a 10× Chromium Single Cell instrument (10x Genomics). This method generated single-cell suspension with greater than 95% viability.

Statistical analysis

For human studies, results are reported as means ± SEM unless otherwise stated. Between-group comparisons for continuous variables were performed by Mann-Whitney test according to a nonparametric distribution (tables S2 and S3). A two-sided *P* value of <0.05 was considered statistically significant.

For animal and in vitro studies, results are reported as means ± SEM unless otherwise stated. The number of mice used, numbers of replicates, and statistical values (where applicable) are provided in the figure legends. Comparison between groups was performed by the Mann-Whitney test or through the analysis of variance (ANOVA) for multiple comparisons (ANOVA for repeated measures) with Bonferroni post hoc analysis. A *P* value of <0.05 was considered statistically significant. Statistical analysis was performed using OriginPro (RRID:SCR_015636) statistical software.

SUPPLEMENTARY MATERIALS

www.science.org/doi/10.1126/scitranslmed.abg3277
Materials and Methods

Figs. S1 to S13
Tables S1 to S3
Data file S1
Movie S1
MDAR Reproducibility Checklist
References (68–79)

View/request a protocol for this paper from *Bio-protocol*.

REFERENCES AND NOTES

1. L. Anguiano, R. Kain, H. J. Anders, The glomerular crescent: Triggers, evolution, resolution, and implications for therapy. *Curr. Opin. Nephrol. Hypertens.* **29**, 302–309 (2020).
2. S. K. Singh, M. Jeansson, S. E. Quaggin, New insights into the pathogenesis of cellular crescents. *Curr. Opin. Nephrol. Hypertens.* **20**, 258–262 (2011).
3. D. Nakazawa, S. Masuda, U. Tomaru, A. Ishizu, Pathogenesis and therapeutic interventions for ANCA-associated vasculitis. *Nat. Rev. Rheumatol.* **15**, 91–101 (2019).
4. M. Segelmark, T. Hellmark, Anti-glomerular basement membrane disease: An update on subgroups, pathogenesis and therapies. *Nephrol. Dial. Transplant.* **34**, 1826–1832 (2019).
5. S. Romoli, M. L. Angelotti, G. Antonelli, S. Kumar Vr, S. R. Mulay, J. Desai, L. Anguiano Gomez, D. Thomasova, D. Eulberg, S. Klussmann, M. E. Melica, C. Conte, D. Lombardi, L. Lasagni, H. J. Anders, P. Romagnani, CXCL12 blockade preferentially regenerates lost podocytes in cortical nephrons by targeting an intrinsic podocyte-progenitor feedback mechanism. *Kidney Int.* **94**, 1111–1126 (2018).
6. L. Lasagni, M. L. Angelotti, E. Ronconi, D. Lombardi, S. Nardi, A. Peired, F. Becherucci, B. Mazzinghi, A. Sisti, S. Romoli, A. Burger, B. Schaefer, A. Buccoliero, E. Lazzeri, P. Romagnani, Podocyte regeneration driven by renal progenitors determines glomerular disease remission and can be pharmacologically enhanced. *Stem Cell Rep.* **5**, 248–263 (2015).
7. S. S. Roeder, T. J. Barnes, J. S. Lee, I. Kato, D. G. Eng, N. V. Kaverina, M. W. Sunseri, C. Daniel, K. Amann, J. W. Pippin, S. J. Shankland, Activated ERK1/2 increases CD44 in glomerular parietal epithelial cells leading to matrix expansion. *Kidney Int.* **91**, 896–913 (2017).
8. H. Lazareth, C. Henique, O. Lenoir, V. G. Puelles, M. Flamant, G. Bollee, C. Fligny, M. Camus, L. Guyonnet, C. Millien, F. Gaillard, A. Chipont, B. Robin, S. Fabrega, N. Dhaun, E. Camerer, O. Kretz, F. Grahammer, F. Braun, T. B. Huber, D. Nochy, C. Mandet, P. Bruneval, L. Mesnard, E. Thervet, A. Karras, F. Le Naour, E. Rubinstein, C. Boucheix, A. Alexandrou, M. J. Moeller, C. Bouzigues, P. L. Tharaux, The tetraspanin CD9 controls migration and proliferation of parietal epithelial cells and glomerular disease progression. *Nat. Commun.* **10**, 3303 (2019).
9. H. Lazareth, O. Lenoir, P. L. Tharaux, Parietal epithelial cells role in repair versus scarring after glomerular injury. *Curr. Opin. Nephrol. Hypertens.* **29**, 293–301 (2020).
10. E. Ronconi, C. Sagrinati, M. L. Angelotti, E. Lazzeri, B. Mazzinghi, L. Ballerini, E. Parente, F. Becherucci, M. Gacci, M. Carini, E. Maggi, M. Serio, G. B. Vannelli, L. Lasagni, S. Romagnani, P. Romagnani, Regeneration of glomerular podocytes by human renal progenitors. *J. Am. Soc. Nephrol.* **20**, 322–332 (2009).
11. E. Lazzeri, M. L. Angelotti, A. Peired, C. Conte, J. A. Marschner, L. Maggi, B. Mazzinghi, D. Lombardi, M. E. Melica, S. Nardi, E. Ronconi, A. Sisti, G. Antonelli, F. Becherucci, L. De Chiara, R. R. Guevara, A. Burger, B. Schaefer, F. Annunziato, H. J. Anders, L. Lasagni, P. Romagnani, Endocycle-related tubular cell hypertrophy and progenitor proliferation recover renal function after acute kidney injury. *Nat. Commun.* **9**, 1344 (2018).
12. B. Smeets, M. L. Angelotti, P. Rizzo, H. Dijkman, E. Lazzeri, F. Mooren, L. Ballerini, E. Parente, C. Sagrinati, B. Mazzinghi, E. Ronconi, F. Becherucci, A. Benigni, E. Steenbergen, L. Lasagni, G. Remuzzi, J. Wetzels, P. Romagnani, Renal progenitor cells contribute to hyperplastic lesions of podocytopathies and crescentic glomerulonephritis. *J. Am. Soc. Nephrol.* **20**, 2593–2603 (2009).
13. H. J. Anders, P. Romagnani, A. Mantovani, Pathomechanisms: Homeostatic chemokines in health, tissue regeneration, and progressive diseases. *Trends Mol. Med.* **20**, 154–165 (2014).
14. A. J. Mead, A. Mullally, Myeloproliferative neoplasm stem cells. *Blood* **129**, 1607–1616 (2017).
15. J. Chen, Y. R. Kao, D. Sun, T. I. Todorova, D. Reynolds, S. R. Narayanagari, C. Montagna, B. Will, A. Verma, U. Steidl, Myelodysplastic syndrome progression to acute myeloid leukemia at the stem cell level. *Nat. Med.* **25**, 103–110 (2019).
16. P. Romagnani, Y. Rinkevich, B. Dekel, The use of lineage tracing to study kidney injury and regeneration. *Nat. Rev. Nephrol.* **11**, 420–431 (2015).
17. M. Schieber, J. D. Crispino, B. Stein, Myelofibrosis in 2019: Moving beyond JAK2 inhibition. *Blood Cancer J.* **9**, 74 (2019).
18. E. Evrot, N. Ebel, V. Romanet, C. Roelli, R. Andraos, Z. Qian, A. Dolemeyer, E. Dammassa, D. Sterker, R. Cozens, F. Hofmann, M. Murakami, F. Baffert, T. Radimerski, JAK1/2 and pan-deacetylase inhibitor combination therapy yields improved efficacy in preclinical mouse models of JAK2V617F-driven disease. *Clin. Cancer Res.* **19**, 6230–6241 (2013).
19. C. Harrison, J. J. Kiladjian, H. K. Al-Ali, H. Gisslinger, R. Waltzman, V. Stalbovskaya, M. McQuitty, D. S. Hunter, R. Levy, L. Knoops, F. Cervantes, A. M. Vannucchi, T. Barbui,

G. Barosi, JAK inhibition with ruxolitinib versus best available therapy for myelofibrosis. *N. Engl. J. Med.* **366**, 787–798 (2012).

20. A. Chen, K. Lee, V. D. D'Agati, C. Wei, J. Fu, T. J. Guan, J. C. He, D. Schlondorff, J. Agudo, Bowman's capsule provides a protective niche for podocytes from cytotoxic CD8$^+$ T cells. *J. Clin. Invest.* **128**, 3413–3424 (2018).

21. A. R. Kitching, M. A. Alikhan, CD8$^+$ cells and glomerular crescent formation: Outside-in as well as inside-out. *J. Clin. Invest.* **128**, 3231–3233 (2018).

22. S. Moll, A. Angeletti, L. Scapozza, A. Cavalli, G. M. Ghiggeri, M. Prunotto, Glomerular macrophages in human auto- and allo-immune nephritis. *Cell* **10**, (2021).

23. D. Odobasic, P. Y. Gan, S. A. Summers, T. J. Semple, R. C. Muljadi, Y. Iwakura, A. R. Kitching, S. R. Holdsworth, Interleukin-17A promotes early but attenuates established disease in crescentic glomerulonephritis in mice. *Am. J. Pathol.* **179**, 1188–1198 (2011).

24. A. R. Kitching, S. R. Holdsworth, P. G. Tipping, Crescentic glomerulonephritis—A manifestation of a nephritogenic T$_H$1 response? *Histol. Histopathol.* **15**, 993–1003 (2000).

25. P. G. Tipping, S. R. Holdsworth, T cells in crescentic glomerulonephritis. *J. Am. Soc. Nephrol.* **17**, 1253–1263 (2006).

26. Y. Luque, D. Cathelin, S. Vandermeersch, X. Xu, J. Sohier, S. Placier, Y. C. Xu-Dubois, K. Louis, A. Hertig, J. C. Bories, F. Vasseur, F. Campagne, J. P. Di Santo, C. Vosshenrich, E. Rondeau, L. Mesnard, Glomerular common γ chain confers B- and T-cell-independent protection against glomerulonephritis. *Kidney Int.* **91**, 1146–1158 (2017).

27. C. D. Pusey, Mechanisms of glomerular crescent formation. *UpToDate* (2020).

28. H. J. Anders, Diagnosis and management of crescentic glomerulonephritis: State of the art. *Saudi J. Kidney Dis. Transpl.* **11**, 353–361 (2000).

29. D. Unnersjo-Jess, L. Scott, H. Blom, H. Brismar, Super-resolution stimulated emission depletion imaging of slit diaphragm proteins in optically cleared kidney tissue. *Kidney Int.* **89**, 243–247 (2016).

30. C. Sagrinati, G. S. Netti, B. Mazzinghi, E. Lazzeri, F. Liotta, F. Frosali, E. Ronconi, C. Meini, M. Gacci, R. Squecco, M. Carini, L. Gesualdo, F. Francini, E. Maggi, F. Annunziato, L. Lasagni, S. Serio, S. Romagnani, P. Romagnani, Isolation and characterization of multipotent progenitor cells from the Bowman's capsule of adult human kidneys. *J. Am. Soc. Nephrol.* **17**, 2443–2456 (2006).

31. S. Safarikia, G. Carpino, D. Overi, V. Cardinale, R. Venere, A. Franchitto, P. Onori, D. Alvaro, E. Gaudio, Distinct EpCAM-positive stem cell niches are engaged in chronic and neoplastic liver diseases. *Front. Med.* **7**, 479 (2020).

32. A. Shiba-Ishii, J. Kano, H. Morishita, Y. Sato, Y. Minami, M. Noguchi, High expression of stratifin is a universal abnormality during the course of malignant progression of early-stage lung adenocarcinoma. *Int. J. Cancer* **129**, 2445–2453 (2011).

33. J. Lin, D. Zhang, Y. Fan, Y. Chao, J. Chang, N. Li, L. Han, C. Han, Regulation of cancer stem cell self-renewal by HOXB9 antagonizes endoplasmic reticulum stress-induced melanoma cell apoptosis via the miR-765-FOXA2 axis. *J. Invest. Dermatol.* **138**, 1609–1619 (2018).

34. S. Bhatlekar, J. Z. Fields, B. M. Boman, Role of HOX genes in stem cell differentiation and cancer. *Stem Cells Int.* **2018**, 3569493 (2018).

35. M. Munz, P. A. Baeuerle, O. Gires, The emerging role of EpCAM in cancer and stem cell signaling. *Cancer Res.* **69**, 5627–5629 (2009).

36. A. J. Peired, G. Antonelli, M. L. Angelotti, M. Allinovi, F. Guzzi, A. Sisti, R. Semeraro, C. Conte, B. Mazzinghi, S. Nardi, M. E. Melica, L. De Chiara, E. Lazzeri, L. Lasagni, T. Lottini, S. Landini, S. Giglio, A. Mari, F. Di Maida, A. Antonelli, F. Porpiglia, R. Schiavina, V. Ficarra, D. Facchiano, M. Gacci, S. Serni, M. Carini, G. J. Netto, R. M. Roperto, A. Magi, C. F. Christiansen, M. Rotondi, H. Liapis, H. J. Anders, A. Minervini, M. R. Raspollini, P. Romagnani, Acute kidney injury promotes development of papillary renal cell adenoma and carcinoma from renal progenitor cells. *Sci. Transl. Med.* **12**, eaaw6003 (2020).

37. E. Lazzeri, M. L. Angelotti, C. Conte, H. J. Anders, P. Romagnani, Surviving acute organ failure: Cell polyploidization and progenitor proliferation. *Trends Mol. Med.* **25**, 366–381 (2019).

38. Y. Dai, A. Chen, R. Liu, L. Gu, S. Sharma, W. Cai, F. Salem, D. J. Salant, J. W. Pippin, S. J. Shankland, M. J. Moeller, N. B. Ghyselinck, X. Ding, P. Y. Chuang, K. Lee, J. C. He, Retinoic acid improves nephrotoxic serum-induced glomerulonephritis through activation of podocyte retinoic acid receptor α. *Kidney Int.* **92**, 1444–1457 (2017).

39. A. Peired, M. L. Angelotti, E. Ronconi, G. la Marca, B. Mazzinghi, A. Sisti, D. Lombardi, E. Giocaliere, M. Della Bona, F. Villanelli, E. Parente, L. Ballerini, C. Sagrinati, N. Wanner, T. B. Huber, H. Liapis, E. Lazzeri, L. Lasagni, P. Romagnani, Proteinuria impairs podocyte regeneration by sequestering retinoic acid. *J. Am. Soc. Nephrol.* **24**, 1756–1768 (2013).

40. P. Romagnani, Toward the identification of a "renopoietic system"? *Stem Cells* **27**, 2247–2253 (2009).

41. K. Sainio, A. Raatikainen-Ahokas, Mesonephric kidney—A stem cell factory? *Int. J. Dev. Biol.* **43**, 435–439 (1999).

42. M. L. Angelotti, E. Ronconi, L. Ballerini, A. Peired, B. Mazzinghi, C. Sagrinati, E. Parente, M. Gacci, M. Carini, E. Rotondi, A. B. Fogo, E. Lazzeri, L. Lasagni, P. Romagnani, Characterization of renal progenitors committed toward tubular lineage and their regenerative potential in renal tubular injury. *Stem Cells* **30**, 1714–1725 (2012).

43. C. C. Estrada, A. Maldonado, S. K. Mallipattu, Therapeutic inhibition of VEGF signaling and associated nephrotoxicities. *J. Am. Soc. Nephrol.* **30**, 187–200 (2019).

44. S. Saw, A. Weiss, R. Khokha, P. D. Waterhouse, Metalloproteases: On the watch in the hematopoietic niche. *Trends Immunol.* **40**, 1053–1070 (2019).

45. H. J. Snippert, A. G. Schepers, J. H. van Es, B. D. Simons, H. Clevers, Biased competition between Lgr5 intestinal stem cells driven by oncogenic mutation induces clonal expansion. *EMBO Rep.* **15**, 62–69 (2014).

46. A. G. Schepers, H. J. Snippert, D. E. Stange, M. van den Born, J. H. van Es, M. van de Wetering, H. Clevers, Lineage tracing reveals Lgr5$^+$ stem cell activity in mouse intestinal adenomas. *Science* **337**, 730–735 (2012).

47. K. K. Youssef, A. Van Keymeulen, G. Lapouge, B. Beck, C. Michaux, Y. Achouri, P. A. Sotiropoulou, C. Blanpain, Identification of the cell lineage at the origin of basal cell carcinoma. *Nat. Cell Biol.* **12**, 299–305 (2010).

48. M. Ryu, A. Migliorini, N. Miosge, O. Gross, S. Shankland, P. T. Brinkkoetter, H. Hagmann, P. Romagnani, H. Liapis, H. J. Anders, Plasma leakage through glomerular basement membrane ruptures triggers the proliferation of parietal epithelial cells and crescent formation in non-inflammatory glomerular injury. *J. Pathol.* **228**, 482–494 (2012).

49. H. Fu, R. R. Subramanian, S. C. Masters, 14-3-3 proteins: Structure, function, and regulation. *Annu. Rev. Pharmacol. Toxicol.* **40**, 617–647 (2000).

50. D. K. Morrison, The 14-3-3 proteins: Integrators of diverse signaling cues that impact cell fate and cancer development. *Trends Cell Biol.* **19**, 16–23 (2009).

51. T. C. Chang, C. C. Liu, E. W. Hsing, S. M. Liang, Y. H. Chi, L. Y. Sung, S. P. Lin, T. L. Shen, B. S. Ko, B. L. Yen, S. F. Yet, K. K. Wu, J. Y. Liou, 14-3-3σ regulates β-catenin-mediated mouse embryonic stem cell proliferation by sequestering GSK-3β. *PLOS ONE* **7**, e40193 (2012).

52. J. Jiang, J. Balcerek, K. Rozenova, Y. Cheng, A. Bersenev, C. Wu, Y. Song, W. Tong, 14-3-3 regulates the LNK/JAK2 pathway in mouse hematopoietic stem and progenitor cells. *J. Clin. Invest.* **122**, 2079–2091 (2012).

53. F. Cianfarani, S. Bernardini, N. De Luca, E. Dellambra, L. Tatangelo, C. Tiveron, C. M. Niessen, G. Zambruno, D. Castiglia, T. Odorisio, Impaired keratinocyte proliferative and clonogenic potential in transgenic mice overexpressing 14-3-3σ in the epidermis. *J. Invest. Dermatol.* **131**, 1821–1829 (2011).

54. X. Fan, L. Cui, Y. Zeng, W. Song, U. Gaur, M. Yang, 14-3-3 proteins are on the crossroads of cancer, aging, and age-related neurodegenerative disease. *Int. J. Mol. Sci.* **20**, (2019).

55. A. Bersenev, C. Wu, J. Balcerek, J. Jing, M. Kundu, G. A. Blobel, K. R. Chikwava, W. Tong, Lnk constrains myeloproliferative diseases in mice. *J. Clin. Invest.* **120**, 2058–2069 (2010).

56. F. Baran-Marszak, H. Magdoud, C. Desterke, A. Alvarado, C. Roger, S. Harel, E. Mazoyer, B. Cassinat, S. Chevret, C. Tonetti, S. Giraudier, P. Fenaux, F. Cymbalista, N. Varin-Blank, M. C. Le Bousse-Kerdiles, J. J. Kiladjian, L. Velazquez, Expression level and differential JAK2-V617F-binding of the adaptor protein Lnk regulates JAK2-mediated signals in myeloproliferative neoplasms. *Blood* **116**, 5961–5971 (2010).

57. S. Grouls, D. M. Iglesias, N. Wentzensen, M. J. Moeller, M. Bouchard, R. Kemler, P. Goodyer, F. Niggli, H. J. Grone, W. Kriz, R. Koesters, Lineage specification of parietal epithelial cells requires β-catenin/Wnt signaling. *J. Am. Soc. Nephrol.* **23**, 63–72 (2012).

58. T. Ulyanova, L. M. Scott, G. V. Priestley, Y. Jiang, B. Nakamoto, P. A. Koni, T. Papayannopoulou, VCAM-1 expression in adult hematopoietic and nonhematopoietic cells is controlled by tissue-inductive signals and reflects their developmental origin. *Blood* **106**, 86–94 (2005).

59. J. Eymael, S. Sharma, M. A. Loeven, J. F. Wetzels, F. Mooren, S. Florquin, J. K. Deegens, B. K. Willemsen, V. Sharma, T. H. van Kuppevelt, M. A. Bakker, T. Ostendorf, M. J. Moeller, H. B. Dijkman, B. Smeets, J. van der Vlag, CD44 is required for the pathogenesis of experimental crescentic glomerulonephritis and collapsing focal segmental glomerulosclerosis. *Kidney Int.* **93**, 626–642 (2018).

60. A. Rambaldi, A. Iurlo, A. M. Vannucchi, R. Noble, N. von Bubnoff, A. Guarini, B. Martino, A. Pezzutto, G. Carli, M. De Muro, S. Luciani, M. F. McMullin, N. Cambier, J. P. Marolleau, R. A. Mesa, R. Tibes, A. Pancrazzi, F. Gesullo, P. Bettica, S. Manzoni, S. Di Tollo, Safety and efficacy of the maximum tolerated dose of givinostat in polycythemia vera: A two-part phase Ib/II study. *Leukemia* **34**, 2234–2237 (2020).

61. J. Mascarenhas, Rationale for combination therapy in myelofibrosis. *Best Pract. Res. Clin. Haematol.* **27**, 197–208 (2014).

62. D. Odobasic, J. R. Ghali, K. M. O'Sullivan, S. R. Holdsworth, A. R. Kitching, Glomerulonephritis induced by heterologous anti-GBM globulin as a planted foreign antigen. *Curr. Protoc. Immunol.* **106**, 15.26.1–15.26.20 (2014).

63. D. Tan, C. Phipps, W. Y. Hwang, S. Y. Tan, C. H. Yeap, Y. H. Chan, K. Tay, S. T. Lim, Y. S. Lee, S. G. Kumar, S. C. Ng, S. Fadilah, W. S. Kim, Y. T. Goh; SGH651 Investigators, Panobinostat in combination with bortezomib in patients with relapsed or refractory peripheral T-cell lymphoma: An open-label, multicentre phase 2 trial. *Lancet Haematol.* **2**, e326–e333 (2015).

64. A. Baggiolini, S. Varum, J. M. Mateos, D. Bettosini, N. John, M. Bonalli, U. Ziegler, L. Dimou, H. Clevers, R. Furrer, L. Sommer, Premigratory and migratory neural crest cells are multipotent in vivo. *Cell Stem Cell* **16**, 314–322 (2015).

65. H. J. Snippert, L. G. van der Flier, T. Sato, J. H. van Es, M. van den Born, C. Kroon-Veenboer, N. Barker, A. M. Klein, J. van Rheenen, B. D. Simons, H. Clevers, Intestinal crypt

Melica *et al.*, *Sci. Transl. Med.* **14**, eabg3277 (2022)   10 August 2022

16 of 17

homeostasis results from neutral competition between symmetrically dividing Lgr5 stem cells. *Cell* **143**, 134–144 (2010).

66. R. L. Mort, M. J. Ford, A. Sakaue-Sawano, N. O. Lindstrom, A. Casadio, A. T. Douglas, M. A. Keighren, P. Hohenstein, A. Miyawaki, I. J. Jackson, Fucci2a: A bicistronic cell cycle reporter that allows Cre mediated tissue specific expression in mice. *Cell Cycle* **13**, 2681–2696 (2014).

67. J. Park, R. Shrestha, C. Qiu, A. Kondo, S. Huang, M. Werth, M. Li, J. Barasch, K. Susztak, Single-cell transcriptomics of the mouse kidney reveals potential cellular targets of kidney disease. *Science* **360**, 758–763 (2018).

68. J. Friedemann, R. Heinrich, Y. Shulhevich, M. Raedle, L. William-Olsson, J. Pill, D. Schock-Kusch, Improved kinetic model for the transcutaneous measurement of glomerular filtration rate in experimental animals. *Kidney Int.* **90**, 1377–1385 (2016).

69. A. Dobin, C. A. Davis, F. Schlesinger, J. Drenkow, C. Zaleski, S. Jha, P. Batut, M. Chaisson, T. R. Gingeras, STAR: Ultrafast universal RNA-seq aligner. *Bioinformatics* **29**, 15–21 (2013).

70. A. T. Lun, K. Bach, J. C. Marioni, Pooling across cells to normalize single-cell RNA sequencing data with many zero counts. *Genome Biol.* **17**, 75 (2016).

71. W. E. Johnson, C. Li, A. Rabinovic, Adjusting batch effects in microarray expression data using empirical Bayes methods. *Biostatistics* **8**, 118–127 (2007).

72. F. A. Wolf, P. Angerer, F. J. Theis, SCANPY: Large-scale single-cell gene expression data analysis. *Genome Biol.* **19**, 15 (2018).

73. L. Haghverdi, A. T. L. Lun, M. D. Morgan, J. C. Marioni, Batch effects in single-cell RNA-sequencing data are corrected by matching mutual nearest neighbors. *Nat. Biotechnol.* **36**, 421–427 (2018).

74. H. Wang, F. Cheng, K. Woan, E. Sahakian, O. Merino, J. Rock-Klotz, I. Vicente-Suarez, J. Pinilla-Ibarz, K. L. Wright, E. Seto, K. Bhalla, A. Villagra, E. M. Sotomayor, Histone deacetylase inhibitor LAQ824 augments inflammatory responses in macrophages through transcriptional regulation of IL-10. *J. Immunol.* **186**, 3986–3996 (2011).

75. A. M. Grabiec, O. Korchynskyi, P. P. Tak, K. A. Reedquist, Histone deacetylase inhibitors suppress rheumatoid arthritis fibroblast-like synoviocyte and macrophage IL-6 production by accelerating mRNA decay. *Ann. Rheum. Dis.* **71**, 424–431 (2012).

76. E. Huarte, M. T. Peel, K. Verbist, B. L. Fay, R. Bassett, S. Albeituni, K. E. Nichols, P. A. Smith, Ruxolitinib, a JAK1/2 inhibitor, ameliorates cytokine storm in experimental models of hyperinflammation syndrome. *Front. Pharmacol.* **12**, 650295 (2021).

77. G. Guo, S. Luc, E. Marco, T. W. Lin, C. Peng, M. A. Kerenyi, S. Beyaz, W. Kim, J. Xu, P. P. Das, T. Neff, K. Zou, G. C. Yuan, S. H. Orkin, Mapping cellular hierarchy by single-cell analysis of the cell surface repertoire. *Cell Stem Cell* **13**, 492–505 (2013).

78. M. I. Dawson, E. Elstner, M. Kizaki, D. L. Chen, S. Pakkala, B. Kerner, H. P. Koeffler, Myeloid differentiation mediated through retinoic acid receptor/retinoic X receptor (RXR) not RXR/RXR pathway. *Blood* **84**, 446–452 (1994).

79. I. Triviai, T. Stubig, B. Niebuhr, K. Hussein, A. Tsiftsoglou, B. Fehse, C. Stocking, N. Kroger, CD133 marks a stem cell population that drives human primary myelofibrosis. *Haematologica* **100**, 768–779 (2015).

Melica et al., Sci. Transl. Med. **14**, eabg3277 (2022)   10 August 2022

17 of 17